

NUMERICAL INVESTIGATION OF HEMODYNAMICS IN THE ARTIFICIAL
ARTERY-AORTA ANASTOMOSIS AND THE INFLOW CANNULA IN
VENTRICULAR ASSIST SYSTEMS TO PREVENT COMPLICATIONS

by
Gizem İnci

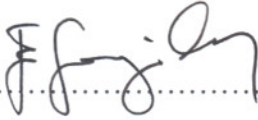
Submitted to the Institute of Graduate Studies in
Science and Engineering in partial fulfillment of
the requirements for the degree of
Master of Science
in
Mechanical Engineering

Yeditepe University
2010

NUMERICAL INVESTIGATION OF HEMODYNAMICS IN THE ARTIFICIAL
ARTERY-AORTA ANASTOMOSIS AND THE INFLOW CANNULA IN VENTRICULAR
ASSIST SYSTEMS TO PREVENT COMPLICATIONS

APPROVED BY:

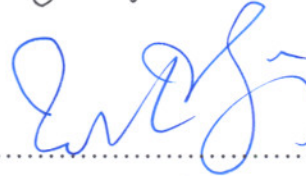
Assist. Prof. Esra Sorgüven Öner
(Supervisor)


.....

Assist. Prof. Levent Kavurmacioğlu


.....

Prof. Dr. Mehmet A. Akgün


.....

DATE OF APPROVAL: 16/06/2010

ACKNOWLEDGEMENTS

First of all, I want to thank Asst. Prof. Esra Sorgüven and Prof. Nilüfer Eğrican, my supporter and adviser throughout my career at Yeditepe University. Prof. Sorgüven gave me the opportunity to work on her projects and introduced me to the fascinating field of computational fluid dynamics. I am really grateful to her for her continual patience and confidence in me. She has been available in every way as a resource, be it emotionally, socially, scholarly, or administratively. I also want to thank to Assoc. Prof. Erdem An, who is most responsible for advising me in Yeditepe University and Esra Sorgüven. Besides my advisor, I want to thank my committee members: Prof. Dr. Mehmet Akgün and Asst. Prof. Levent Kavurmaciođlu. I appreciate their advice, comments, suggestions, time, and encouragement. Last, but not least, I thank my family: my parents, my sister, for their unconditional support and encouragement. And a special thanks to all my friends, and Fahri Dikbař, for listening my complaints and frustrations, and for believing in me.

This study was funded by TUBITAK, The Scientific and Technical Council of Turkey, through the research grant no: 108M377.

ABSTRACT

NUMERICAL INVESTIGATION OF HEMODYNAMICS IN THE ARTIFICIAL ARTERY-AORTA ANASTOMOSIS AND THE INFLOW CANNULA IN VENTRICULAR ASSIST SYSTEMS TO PREVENT COMPLICATIONS

Cardiovascular diseases are the most frequent cause of fatality among older populations. Congestive heart failure makes up a considerably large portion of cardiovascular diseases. Ventricular assist devices, which have an increasing success rate in clinical applications, are used to solve these problems. But even with optimized heart pumps fatal complications can occur because of the deformations around the inflow cannula or through the artificial artery – aorta anastomosis. Due to high rotational speeds of heart pumps, blood cells pass through the pump rapidly and usually without undergoing any deformation. As blood cells flow from the left ventricle into the inflow cannula, flow velocity decreases and reverse flow zones occur, both of which may lead to hemolysis and thrombosis. Similarly, the change in the hemodynamics through the artificial artery – aorta anastomosis causes deformation of blood cells and endothelium. To investigate the inflow cannula of heart pumps and the artificial artery – aorta anastomosis and possible clinical consequences, in order to decrease complications and increase the success rate of ventricular assist devices, which is a very difficult and expensive therapy option, computational fluid dynamics analysis were performed using patient-specific geometrical models and boundary conditions. The simulations indicate that the positions of the anastomosis and the cannula have important effects on flow. CFD results provide insight on the altered hemodynamics in the aforementioned regions.

ÖZET

VENTRİKÜLER DESTEK SİSTEMLERİNDE KOMPLİKASYONLARIN AZALTILMASI AMACIYLA YAPAY DAMAR – AORTA ANASTOMOZUNUN VE GİRİŞ KANÜLÜNÜN HEMODİNAMİK AÇIDAN SAYISAL İNCELENMESİ

Kalp damar hastalıkları özellikle orta-ileri yaş gruplarında en sık rastlanan ölüm sebebidir. Kalp yetmezliği ise bu ölümlerin büyük bir kısmını oluşturur. Klinik uygulamada başarı oranı giderek artan ventriüler destek sistemleri kalp yetmezliği tedavisinde kullanılmaktadır. Kalp pompası optimize edilmiş sistemlerde bile hastalar, giriş kanülü etrafında ya da pompa çıkışının aortaya bağlandığı bölgede oluşan komplikasyonlar sebebiyle kaybedilebilmektedir. Kalp pompası yüksek devirlerde çalıştığından, kan hücreleri hızla ve parçalanmadan pompadan geçmekte, ancak sol ventrikülden pompa giriş kanülüne doğru akış hızı yavaşlayıp, ters akış bölgeleri oluştuğundan hemoliz ve pıhtı oluşumu gözlenebilmektedir. Benzer bir şekilde pompa çıkışındaki yapay damar ile aorta anastomozu bölgesinde hemodinamik yapının değişmesi kan hücrelerinin yıkımına ve damar iç yüzeyinin yıpranmasına yol açmaktadır. Bu çalışmada, pahalı ve zor bir tedavi yöntemi olan ventriküler destek sistemlerinin uygulamalarında karşılaşılan komplikasyonları azaltmak ve başarı oranını artırmak için kalp pompası giriş kanülü ve yapay damar – aorta anastomoz bölgeleri sayısal olarak incelendi. Hesaplamalı akışkanlar dinamiği metodu kullanılarak yapılan simülasyonlarda gerçeğe uygun sol karıncık ve aort geometrileri ve gerçeğe uygun ve sınır koşulları kullanıldı. HAD metodu simülasyon sonuçları, anastomoz bağlantısının ve kanül geometrisinin kan akışına etkilerini göstermekte ve incelenen bölgelerde hemodinamik değişim bilgisi vermektedir.

TABLE OF CONTENTS

ACKNOWLEDGEMENTS.....	iii
ABSTRACT.....	iv
ÖZET	v
TABLE OF CONTENTS.....	vi
LIST OF FIGURES	viii
LIST OF TABLES	xii
LIST OF SYMBOLS/ABBREVIATIONS.....	xiii
1. INTRODUCTION	1
1.1. MOTIVATION.....	1
1.2. HEMODYNAMICS.....	3
1.3. COMPUTATIONAL FLUID DYNAMICS	4
1.4. OBJECTIVES	6
2. BACKGROUND.....	7
2.1. CONGESTIVE HEART FAILURE	7
1.1.1. Causes	7
1.1.2. Treatment	8
2.2. BLOOD AND BLOOD PRESSURE.....	9
2.3. ANASTOMOSIS.....	11
3. MEDICAL IMAGES AND GEOMETRIE CONSTRUCTION.....	13
3.1. COMPUTED TOMOGRAPHY IMAGES	14
3.2. MAGNETIC RESONANCE IMAGES.....	16
3.3. CAD GEOMETRIES	19
3.3.1. Aorta.....	20
3.3.2. Aorta-Artificial Artery Anastomosis.....	21
3.3.3. Left Ventricle and Cannula	27
4. FLOW INSIDE THE NATIVE AORTA.....	30
4.1. LITERATURE SURVEY	30
4.2. GEOMETRY AND MESH	30
4.2.1. Law of Wall Functions.....	34
4.2.2. Kolmogorov’s Scale.....	35

4.3. MESH INDEPENDENCY	36
4.4. CFD ANALYSIS	41
4.4.1. Steady, Constant Mass Flow rate	42
4.4.2. Unsteady, Pulsatile Mass Flow rate	44
4.5. CONCLUSION	50
5. AORTA-ARTIFICIAL ARTERY ANASTOMOSIS.....	52
5.1. LITERATURE SURVEY	52
5.2. GEOMETRY AND MESH	53
5.3. TURBULENCE MODELLING TEST	54
5.4. CFD ANALYSIS	55
5.4.1. Steady, Constant Mass Flow rate	56
5.5. CONCLUSION	69
6. LEFT VENTRICLE AND CANNULA.....	70
6.1. LITERATURE SURVEY	70
6.2. GEOMETRY AND MESH	70
6.3. CFD ANALYSIS	71
6.3.1. Steady, Constant Mass Flow Rate.....	72
6.4. CONCLUSION	73
REFERENCES	74
APPENDIX A.....	81

LIST OF FIGURES

Figure 2.1. The circulation of blood through the human heart	10
Figure 2.2. Sketch of end-to-side anastomosis construction from Grevious et al. (2003)...	12
Figure 2.3. Sketch of end-to-end anastomosis	12
Figure 3.1. 2D CT scan slices, right view, left view, top view and perspective.....	14
Figure 3.2. 3D view of patient specific anatomy and 3D smooth view of patient specific aorta.....	15
Figure 3.3. Aorta, left and right ventricle anatomy for second patient.....	16
Figure 3.4. 2D MRI data, magnitude & phase.....	17
Figure 3.5. Time dependent volumetric flow rate on defined ROI.....	18
Figure 3.6. 3D time-resolved flow information through aorta	19
Figure 3.7. Aorta stl geometry	20
Figure 3.8. Aorta CAD geometry cross-section	21
Figure 3.9. Conduit angle on the transversal plane.....	22
Figure 3.10. Conduit insertion angle on the coronal plane	23
Figure 3.11. Artificial artery-aorta anastomosis design with 120° location angle and 60° connection angle	24

Figure 3.12. Artificial artery-aorta anastomosis design with 90° location angle and 30° connection angle	24
Figure 3.13. Artificial artery-aorta anastomosis design with 100° location angle and 15° connection angle	25
Figure 3.14. Design modification	26
Figure 3.15. Artificial artery length	26
Figure 3.16. New artificial artery-aorta anastomosis design	27
Figure 3.17. Leftt ventricle and aorta .stl file and left ventricle cross-section	28
Figure 3.18. CAD design for left ventricle	28
Figure 3.19. Left ventricle and cannula design.....	29
Figure 4.1. Aorta geometry that was used in CFD analysis	31
Figure 4.2. Block structure for O-grid type mesh.....	33
Figure 4.3. Different number of control volumes for 4 test cases; A) 72000, B) 550000, C) 2000000, and D) 5000000.....	37
Figure 4.4. Velocity sections	38
Figure 4.5. Velocity vectors on the section-1	39
Figure 4.6. Velocity vectors on the section-2	40
Figure 4.7. Velocity vectors on section-3	41

Figure 4.8. Pressure distribution on aorta wall	42
Figure 4.9. WSS distribution on aorta wall	43
Figure 4.10. Velocity vectors through aorta	44
Figure 4.11. Lagrange interpolation equations graph	45
Figure 4.12. Pulsatile flow waveform derived from MATLAB code for Lagrange interpolation equation	46
Figure 4.13. MRI and MATLAB flow waveform	47
Figure 4.14. Time dependent pulsatile mass flow rate graph from FLUENT simulation ...	48
Figure 4.15. Velocity vectors (m/s) of time dependent unsteady CFD simulation	49
Figure 4.16. MRI flow patterns	51
Figure 5.1. Velocity streamlines inside conduit and aorta measured from conduit inlet and aorta inlet.....	57
Figure 5.2. Pressure distribution on vessel walls.....	59
Figure 5.3. Max. pressure value on aorta wall.....	60
Figure 5.4. Wall shear stress distribution on vessel walls	61
Figure 5.5. Sections	62
Figure 5.6. Velocity vectors on section-0	63
Figure 5.7. Velocity vectors on section-1	65

Figure 5.8. Velocity vectors on section-3	66
Figure 5.9. Velocity vectors on section-4	68
Figure 6.1. Control volume structure for left ventricle and cannula geometry	71
Figure 6.2. Pressure distribution on middle section.....	72
Figure 6.3. Velocity vectors on middle section	72
Figure A.1. Matlab Code for Lagrange Interpolation formulation	81

LIST OF TABLES

Table 2.1. Blood pressure levels in adults (in mmHg)	11
Table 4.1. Law of wall functions	34
Table 5.1. Different viscous model simulation results	54

LIST OF SYMBOLS/ABBREVIATIONS

C_f	Skin friction coefficient
F	External force per unit mass
K_H	Heat conduction coefficient
mmHg	Millimeter mercury
P	Pressure
Re	Reynolds number
T	Temperature
u	Velocity vector
U_0	Mean velocity
U^*	Friction velocity
y^+	The cell distance from the wall
ε	Thermodynamic internal energy
η	Kolmogorov's length scale
μ	Viscosity
ν	Kinematic viscosity
ρ	Density
τ_η	Kolmogorov's time scale
τ_w	Shear stress
CFD	Computational Fluid Dynamics
CHF	Congestive Heart Failure
CT	Computed Tomography
CV	Control volume
CVD	Cardiovascular Diseases
HAD	Hesaplmalı Akışkanlar Dinamiği
LVAD	Left Ventricle Assist Device
MRI	Magnetic Resonance Imaging
ROI	Region of Interest
RVAD	Right Ventricle Assist Device
VAD	Ventricular Assist Device
WSS	Wall Shear Stress

1. INTRODUCTION

1.1. MOTIVATION

Heart is the life sustaining organ, which is only fist size. It consists of muscular tissue, and its urgent task is to pump the blood throughout the vessels to the tissues of the body by repeated, rhythmic contractions, without a rest during lifetime. The heart is also related with conveying the hormones to the body and helps maintaining body temperature.

According to the importance of the heart functions, one of the most significant criteria is a healthy heart for a quality life. Nevertheless, the cardiovascular diseases are the primarily killer among other diseases, such that cardiovascular diseases caused 16.7 million, or %29.2 of total global deaths all over the world in 2003. In 2005, this value jumped up to about 17 million, which represents 30% of all global deaths and by 2015 it is assumed that cardiovascular diseases will be leading the cause of death [1]. Besides being a major contributor to morbidity and mortality worldwide, cardiovascular heart diseases also affect the daily life activities [2, 3].

Cardiovascular diseases (CVD) are the combination of the diseases that affect heart or blood vessels [4]. CVD's can be classified according to the situations of affecting the structures or function of the heart. They are; (i) coronary artery disease, which is a disease of coronary arteries that supply heart muscles, (ii) abnormal heart rhythm or arrhythmia that is an abnormal electrical activity in the heart, (iii) heart valve disease that occurs when the heart's valves do not work properly, (iv) congenital heart disease that refers to a problem with the structure and function of the heart due to abnormal development before birth, (v) heart attack, which occurs when blood flow to the heart muscle is completely blocked, and (vi) heart failure means the heart is losing its ability to pump blood effectively. These illnesses afflict one individual, however affect entire humanity. The major treatment method for all these diseases is prevention by adjusting diet habits, physical activity levels and tobacco consumption. But when a patient is diagnosed as having cardiovascular diseases, the treatment options must be at the top of the agenda.

In recent years, due to the development in all areas of science, multidisciplinary studies have become more important. There exists significant improvements in biomedical along with pharmaceutical industry, molecular and cell biology. Biomedical researches recognize that the cardiovascular diseases are affected directly by the structure of the heart and blood force and pressure on vessels. Moreover to discover those effects deeply, scientists study in collaboration and try to find new clarifications. Concordantly, new mathematical models, numerical fluid mechanics models especially computational fluid dynamics (CFD), experimental fluid mechanics models, and medical imaging methods are discovered. Most important techniques are those which would combine all these models and methods. Various cardiovascular diseases are recognized with the help of these methods, such that, mathematical models are used to express blood vessels as an electric circuit and control the cardiovascular system [5, 6, 7], patient specific heart and vessel pathologies are detected and blood flow within the cardiovascular system is evaluated from medical images [8, 9, 10], and numerical and/or experimental blood flow analysis are performed on these geometries for bypass graft anastomosis, internal carotid aneurysm [11]. Abdominal aortic aneurysm diseases, atherosclerosis in the carotid artery are studied [12, 13, 14], flow simulations during systolic and diastolic phases of the left ventricle are modeled [15, 16] .etc. Despite being assister to medicine, nowadays these methods are used as prognosis tools and treatment techniques on its own; thereby the medicine is not the only treatment method alone.

Congestive heart failure is one of the most important types of cardiovascular diseases that affect more than 14 million people worldwide. From 1979 to 2004, the number of hospitalized patients increased from 400,000 to 1.1 million, according to the US Centers for Disease Control and Prevention. Thus, this patient group represents an increasing cost, which in the USA is estimated to be between \$20 000 and 40 000 million annually [17]. Also a Swedish study estimated the total annual treatment cost to be SEK 2000-2600 million, corresponding to nearly 2% of the Swedish healthcare budget [18].

Therefore, to support patients who are at end-stage heart failure, the ventricular assist devices are used. Although the clinical success of these devices increase day by day, approving long-term patient outcome after surgery is adversely affected by hemodynamic changes affecting the heart. Even with optimized devices, some other lethal complications

can occur due to the deformations through the aorta-artificial artery anastomosis and cannula. In order to increase the performance of VADs as well as to anticipate complications that could occur, a myriad of studies have been done [19, 20, 21, 22]. Besides including advantages and disadvantages, with the help of this treatment option, both the life time and life quality are increased for whom having cardiovascular diseases especially heart failure.

In general, to achieve the clinical success in terms of reducing the flow abnormalities and obtaining uniform flow fields at the inlet and at the outlet of the pump as well as the flow through the pump, numerical researches were applied. Different aorta-artificial artery anastomosis configurations and cannula geometry were modeled with the patient specific aorta and left ventricle geometry and computational fluid dynamics (CFD) simulations were performed. The LVAD outflow conduit was added on the ascending aorta and both the location and the insertion angle of the artificial artery within 18 different designs having the same boundary conditions and mesh blocks and the flow inside left ventricle with cannula geometry were investigated.

1.2. HEMODYNAMICS

The circulatory system is a connected series of tubes, which includes the heart, the arteries, the microcirculation, and the veins. The heart is the driver of this huge system by enabling the blood to move around the body inside the vessels at every heart beat. The study of the blood forces that the heart has to provide is hemodynamics, which is an important subject of cardiovascular physiology that hemodynamic forces are demonstrated as blood pressure and blood flow paired values at different nodes of the cardiovascular systems. For cardiovascular health, longevity and quality of life, adequate supply of oxygen to all tissues is important, therefore this condition can be satisfied only by a uniform and adequate blood flow through the uniform vessels.

Since 1900's, the researchers have been recognized that there is a significant effect of vessel pathology and therefore blood flow on the cardiovascular diseases. Hemodynamic factors that have been suggested to be important in cardiovascular diseases are derived from the velocity field and involve different forms, such as flow separation,

vortex formation and wall shear stress. Vorticity within the flow is computed from velocity field. Wall shear stress (WSS) which includes a micro environment of frictional force between blood and vessel wall is a vector field, and its magnitude is defined as the blood viscosity and flow velocity gradient normal to surface. Wall shear stress is mostly calculated from the local velocity distribution near the wall as it is difficult to compute directly.

Blood has a uniform flow inside a uniform vessel, but secondary flows and reverse flows can be seen through arches and bifurcations however any change on the blood flow, non-uniform flow cause an death of blood cells, in return, which cause thrombosis and hemolysis of the cells.

1.3. COMPUTATIONAL FLUID DYNAMICS

The most important struggle for human beings has been being alive. For this reason most of the scientists deal with all areas of medicine, and for others, any of the health problems always attract them and try to find solutions. So far many mathematical, physical and chemical equations are defined, mechanical and electrical devices are designed and computational technologies are used.

CFD simulations result from numerical solutions of differential equations derived from physical conservation laws for flows. The fundamental bases of almost all CFD problems are the Navier–Stokes equations, which define any single-phase fluid flow satisfying three basic conservation principles. The first principle is the conservation of mass, defined as continuity equation. The second principle is the conservation of momentum, defined as momentum equation, and the third equation is energy equation, which arises from conservation of energy.

$$\frac{\partial \rho}{\partial t} + \nabla \cdot (\rho u) = 0 \quad (1.1)$$

$$\frac{\partial u}{\partial t} + (u \cdot \nabla)u = -\frac{1}{\rho} \nabla p + F + \frac{\mu}{\rho} \nabla^2 u \quad (1.2)$$

$$\rho \left(\frac{\partial \varepsilon}{\partial t} + u \cdot \nabla \varepsilon \right) - \nabla \cdot (K_H \nabla T) + p \nabla \cdot u = 0 \quad (1.3)$$

$$\nabla = \frac{\partial}{\partial x} \mathbf{i} + \frac{\partial}{\partial y} \mathbf{j} + \frac{\partial}{\partial z} \mathbf{k} \quad (1.4)$$

$$\nabla^2 = \frac{\partial^2}{\partial x^2} + \frac{\partial^2}{\partial y^2} + \frac{\partial^2}{\partial z^2} \quad (1.5)$$

Continuity equations are obtained for conservation of mass (1.1), conservation of momentum (1.2) and conservation of energy (1.3).

Succeeding new developments in computer technology, new procedures have been used in medicine since 1900's [22, 23, 24, 25, 26, 27]. Especially for cardiovascular systems, as the "blood" is one of the most important parts of this system, computational fluid dynamics (CFD) analysis have been used very widely and effectively [22, 28, 29]. The clinical and experimental techniques have disadvantages in researching blood hemodynamics according to their practical difficulties and financial burdens; however CFD has been proven to be a reliable technique for investigating time-varying, 3D flow patterns in a complex geometrical model. Therefore, computational fluid dynamics simulation of hemodynamics is on the forefront of research of biological flows.

CFD simulations provide additional information of the hemodynamics, present some answers to the questions concerning blood flow and have potential in aiding the therapeutic decision making process. Providing real situations for CFD analysis with accurate boundary conditions and geometry, the simulation results are desirable to obtain with high resolution, which also increase the popularity of CFD for hemodynamic research.

As mentioned, for observing realistic results of blood flow, the CFD analysis should be performed as real cases. These conditions increase the importance of both the geometrical model and boundary conditions, and in that point the medical image data step in. Commercial availability of CFD software, ability to present velocity distributions for blood flow and extract WSS and other hemodynamic factors realistically, results in CFD to be preferred in treatment planning and therapeutic decision making in addition to clinically imaging.

1.4. OBJECTIVES

The aim of this project is to decrease the fatal complications in the ventricular assist devices applications. These complications can occur because of the deformations around the inflow cannula or through the artificial artery – aorta anastomosis. For this purpose, starting from clinical researches, with the help of computational fluid dynamics, the flow through the aorta-artificial artery anastomosis and the inflow cannula will be investigated.

The flow through the ventricular assist device inflow cannula and the artificial artery-aorta anastomosis is simulated to explore deformations of the blood cells and the effects of the anastomosis structure on the flow to find the best anastomosis position that can provide maximum performance in clinical practice. Therefore, to achieve these aims a working strategy was defined including;

- Using patient-specific geometries rather than simple models to provide accurate results.
- Performing numerical solutions considering different anastomosis geometries using both steady and pulsatile flow cases.
- Considering the influence of hemodynamic factors.
- Validating the computational results with literature searches and clinical information.

2. BACKGROUND

2.1. CONGESTIVE HEART FAILURE

The heart is a muscular organ and serves as the pump: to move blood to the body with arteries, carrying nutrients and oxygen to the tissues, and from the body with veins, removing waste products. To continue on a healthy life, body needs this system to work properly, and the amount of required blood flow changes with respect to person's daily activities. More blood flow is required during exercise or times when during greater demands are placed on the body [30].

When the heart loses its ability to pump blood properly means it is not working as sufficient as it should, either during exercise or at rest. This has a negative effect on many bodily functions. Because a weakened heart moves less blood with each pump, fluids backs up in the lungs. As a result, the body does not receive enough oxygen. This condition is named as "heart failure". As mentioned before, heart failure does not mean that the heart fails, and never works, it only does not work as well as it should and the term congestive, comes from congestion, arises in which reduced heart function is accompanied by a buildup of body fluid in the lungs and elsewhere.

The primary signs and symptoms of all types of heart failure include tachycardia, decreased exercise tolerance, shortness of breath, peripheral and pulmonary edema, and cardiomegaly. Congestive heart failure is a progressive, chronic disease, it is a long-term condition and it will worsen over time unless it is treated.

2.1.1. Causes

Heart failure is a syndrome with multiple causes that may involve the right ventricle, left ventricle, or both. Two major types of failure may be distinguished, as systolic failure and diastolic failure. In systolic failure, the mechanical pumping action and the ejection fraction of the heart are reduced; the heart does not efficiently pump blood from the

ventricles to the body. Diastolic heart failure happens when the heart cannot properly fill with blood. In diastolic failure stiffening and loss of adequate relaxation plays a major role in reducing cardiac output and ejection fraction may be normal.

Many things can lead to heart failure. Systolic heart failure is generally affected by a heart attack and persistent high blood pressure. Diastolic heart failure may be a result of systolic heart failure, dysfunctional heart valves, or a diseased heart lining. Although there are other major risk factors, such that diabetes mellitus high cholesterol, obesity, and smoking, the most frequent risk factor is hypertension, also called high blood pressure.

2.1.2. Treatment

When a person is diagnosed as having a CHF, it is important to immediately start treatment. Historically, the number one treatment option is drugs; however for later stages of the illness, drugs may not be sufficient. According to the severity of the condition other treatment options should be revived including heart transplantation, artificial organs or ventricle assist devices.

Currently the cardiac transplantation, in which the damaged or diseased heart is replaced with a healthy one, is the only established treatment method that supplies a substantial survival benefit. It is a surgical transplant process performed on end-stage heart failure patients and the working heart is taken from a donor who has died. From the first heart transplantation operation in 1960s, to today, there have been great improvements in the medical field and in this regard. However, all around the world patients are facing a big problem that is the growing disparity between the number of donor hearts needed for transplantation and the number of available for donation. As the demand for donor hearts is greater than the supply, the waiting lists increase and, in result, important number of patients die [31, 32].

According to disadvantages of heart transplantation, new alternatives to cardiac transplantation is developing, such that total artificial hearts and ventricular assist devices. Ventricular assist devices are mechanical pump-type devices that are used for improving

the function of the failing left heart. They can support the left ventricle (LVAD) or right ventricle (RVAD) alone or both (bi-VAD). They may be used in different categories as;

- Bridge to transplant for the patients, who need support during waiting period.
- Bridge to recovery to supply a recovery option for the heart.
- Destination therapy for the patients for whom cardiac transplant is not an option. Ventricle assist devices are used to give a chance to the patient by improving quality of life and extending life.

There have been important developments in many aspects of VADs, such as reducing the weight, increasing the battery life and enabling the device control, which in turn increase the implantation rates [22, 33]. With these improvements of the assist devices, they are planned to become alternatives to allogenic transplantation in the near future.

2.2. BLOOD AND BLOOD PRESSURE

Blood is a unique bodily fluid, delivers oxygen and nutrients to the body's cells and transports waste products away from those cells flowing through the vessels. Blood is composed of blood plasma and blood cells. Plasma, takes part a more amount about 55% of blood, and it consists of dissolved proteins, glucose, mineral ions, hormones, carbon dioxide and platelets, and 90% by volume of plasma is water. Blood cells present in the blood fluid in the form of red blood cells which are more abundant cells, contain hemoglobin and an iron-containing protein and white blood cells including leukocytes and platelets.

Figure 2.1 shows the blood circulation around the body through blood vessels by the pumping action of the heart. In humans, blood is pumped from the strong left ventricle of the heart through arteries to peripheral tissues and carries oxygen and returns to the right atrium of the heart through veins with carbon dioxide and waste product. It then enters the right ventricle and is pumped through the pulmonary artery to the lungs and returns to the left atrium through the pulmonary veins. Blood then enters the left ventricle to be circulated again.

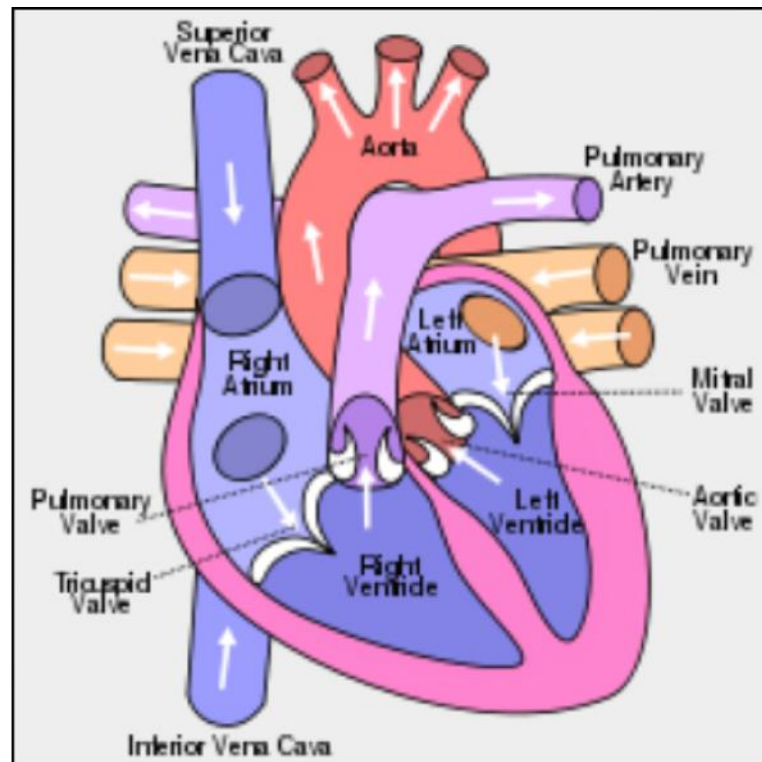


Figure 2.1. The circulation of blood through the human heart

The force that the blood is pushing against the walls of the vessel is blood pressure. Each time the heart beats (about 60-70 times a minute at rest), it pumps out blood into the arteries and the blood pressure is at its highest when the heart beats, pumping the blood. This is called systolic pressure. When the heart is at rest, between beats, the blood pressure falls and this is the diastolic pressure. Therefore, blood pressure is always given as these two numbers, the systolic and diastolic pressures. Usually they are written one above or before the other, such as 120/80 millimeter mercury, where the top number is the systolic and the bottom the diastolic. When the two measurements are written down, the systolic pressure is the first or top number, and the diastolic pressure is the second or bottom number (for example, 120/80).

Table 2.1. Blood pressure levels in adults (in mmHg)

Category	Systolic	Diastolic
Normal	Less than 120	Less than 80
Prehypertension	120-139	80-89
High Blood Pressure	Systolic	Diastolic
Stage 1	140-159	90-99
Stage 2	160 or higher	100 or higher

Blood pressure changes during the day. It is lowest at sleeping and resting and rises when get up and it also can rise when you are excited, nervous, or active.

2.3. ANASTOMOSIS

Anastomosis is a surgical procedure, applied to connect two ducts or blood vessels using a natural vessel or synthetic graft (artificial artery) to allow a continuous channel that blood can flow from one to the other. Clinically two kinds of anastomosis operations are available, as end-to-end anastomosis and end-to-side anastomosis.

End-to-side anastomosis method can be used for both smaller and larger vessels. It is a connection of the end of a one vessel to the side of a larger one.

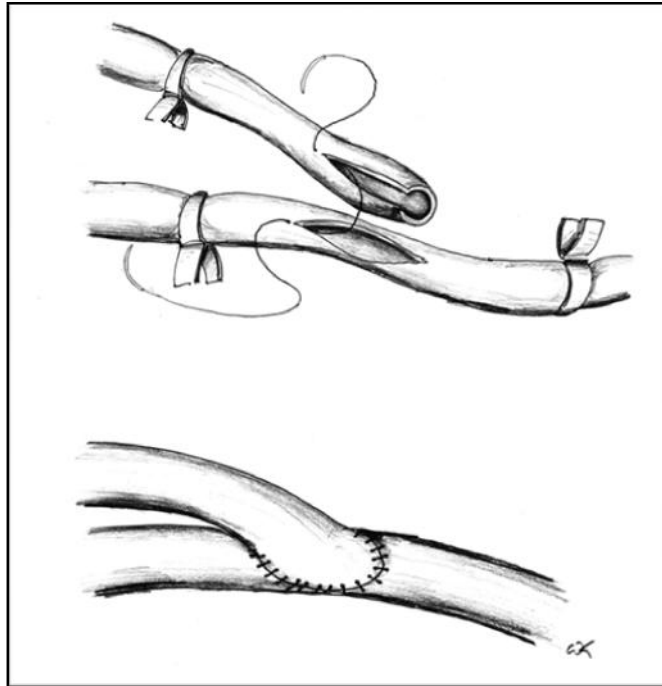


Figure 2.2. Sketch of end-to-side anastomosis construction from Grevious et al. (2003)

End-to-end anastomosis surgery is generally used for large vessels. In this method, in Figure 2.3, the end of the one vessel is connected to the end of other vessel.

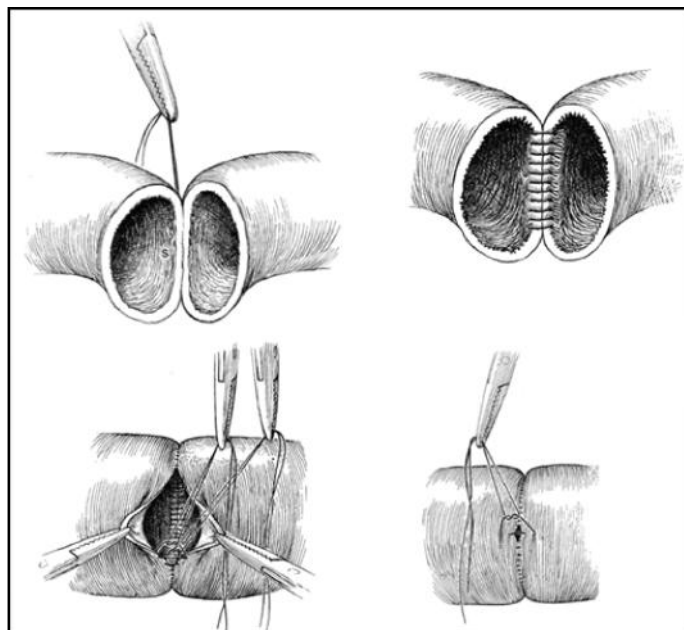


Figure 2.3. Sketch of end-to-end anastomosis

3. MEDICAL IMAGES AND GEOMETRIE CONSTRUCTION

Today medical images are used not only as diagnosing tools but also as treatment options [34, 35]. They allow seeing the patient's pathology, measure physical fields such as blood flow rate, pressure, heart beating rate, and so on. The use of cardiac imaging enables a good assessment of blood dynamics. Also according to the developments in this area, there have been important improvements in clinical studies, so that with using patient-specific systems the treatment options can be more specific and sufficient. The main components of medical images for the cardiovascular systems are computed tomography (CT) to define the anatomy and magnetic resonance imaging (MRI) to define the flow information.

Computed tomography is generally used in the evaluation of the aorta because of its high diagnostic accuracy for detection of aortic pathology. Despite including some hazardous effects on the patient such that ionizing radiation and nephrotoxicity of contrast agents, computed tomography technique is widely available according to its cost-effectiveness and efficiency [36].

Magnetic resonance imagers have used quantitative flow measurements since 1980s, and since 1960 it is potential have been known [37, 38]. Magnetic resonance is an important alternative technology for pre-procedural imaging, where phase contrast imaging is a unique MR technique. It can measure blood flow so it is used in many clinical applications to estimate hemodynamic properties of blood [36]. Magnetic resonance mapping is based on the determination of the acquired phase shift of proton spins moving along a magnetic field gradient. The average velocity in each image was calculated as the average of the pixel values of all pixels within the defined cross-section.

3.1. COMPUTED TOMOGRAPHY IMAGES

To view anatomy of the patient and to construct aorta geometry, 2D CT scans were taken from a 65 years old male patient who was conducted a bypass surgery before; there were about 500 slices with a distance of 0.625 mm.

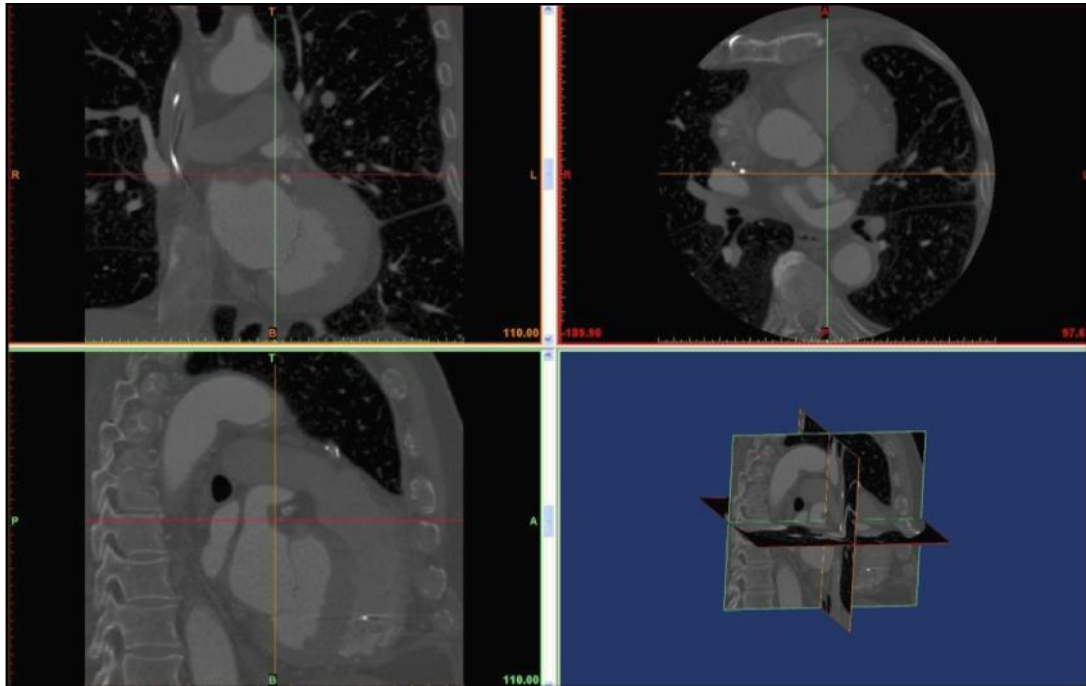


Figure 3.1. 2D CT scan slices, right view, left view, top view and perspective

A commercial code called MIMICS (Materialise Software) was used to reconstruct 3D patient specific anatomy from CT by combining these sequential slices.

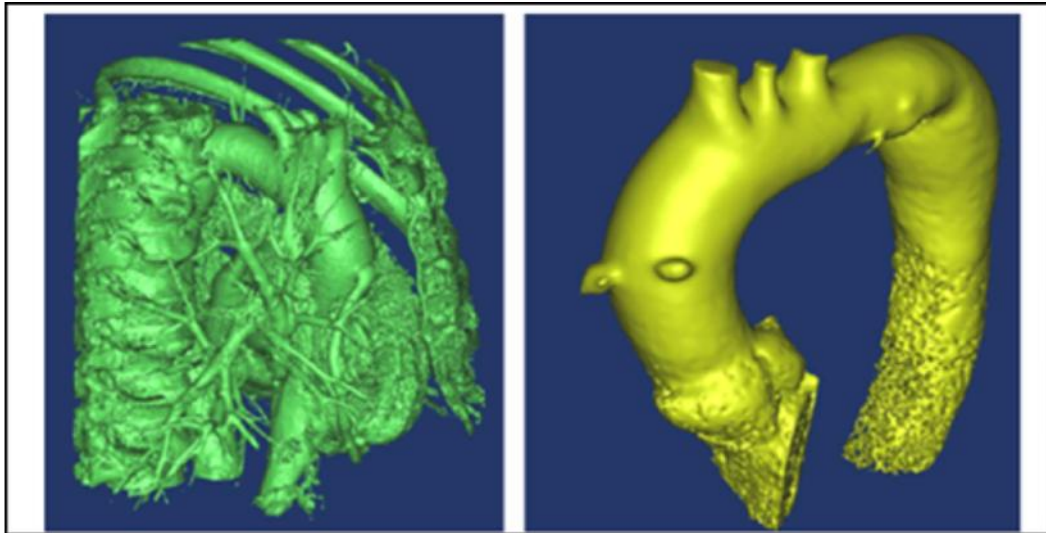


Figure 3.2. 3D view of patient specific anatomy and 3D smooth view of patient specific aorta

Figure 3.2 shows this patient's tomography, which gave only information for aortic valves, aorta, back bone and ribcage, smaller vessels leaving from aorta and the bypass surgery places that the patient had before. This bypass places were taken as reference points for anastomosis positions.

To construct left ventricle geometry, 2D CT scans were taken from a patient who was diagnosed as having heart failure disease before. This patient's tomography data includes both aorta and left and right ventricle geometries (Figure 3.3). Also it had information about patient's end diastolic and end systolic volume values.

- End Diastolic Volume : 290.9 ml
- End Systolic Volume : 247.8 ml
- Stroke Volume : 43.1 ml



Figure 3.3. Aorta, left and right ventricle anatomy for second patient

3.2. MAGNETIC RESONANCE IMAGES

2D and 3D MRI data was taken from 5 different healthy volunteers. 2 of them are 2D MRI data, which contains only one 2D slice on the ascending aorta above the aortic valves including time dependent flow information normal to that surface and anatomy. The first image resembles a normal bright blood image, represents anatomic orientation. The second image represents the velocity information in that voxel with the gray value of each pixel Figure 3.4.

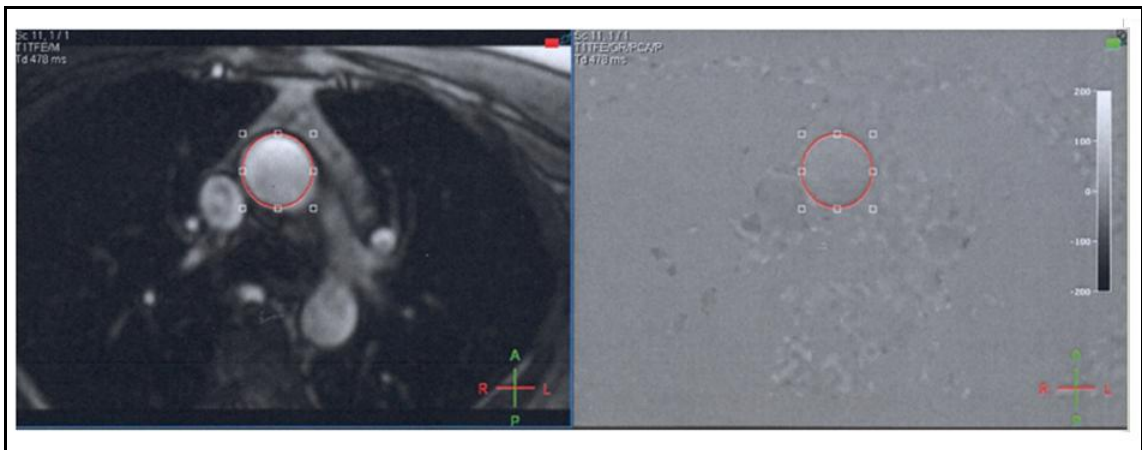


Figure 3.4. 2D MRI data, magnitude & phase

The red circle defines the aorta boundary, called region of interest (ROI). The first picture gives information about the geometry, and the second gray-scale picture gives information about the volumetric flow rate. The points on the 2D flow graph, mark times where the measurements were taken.

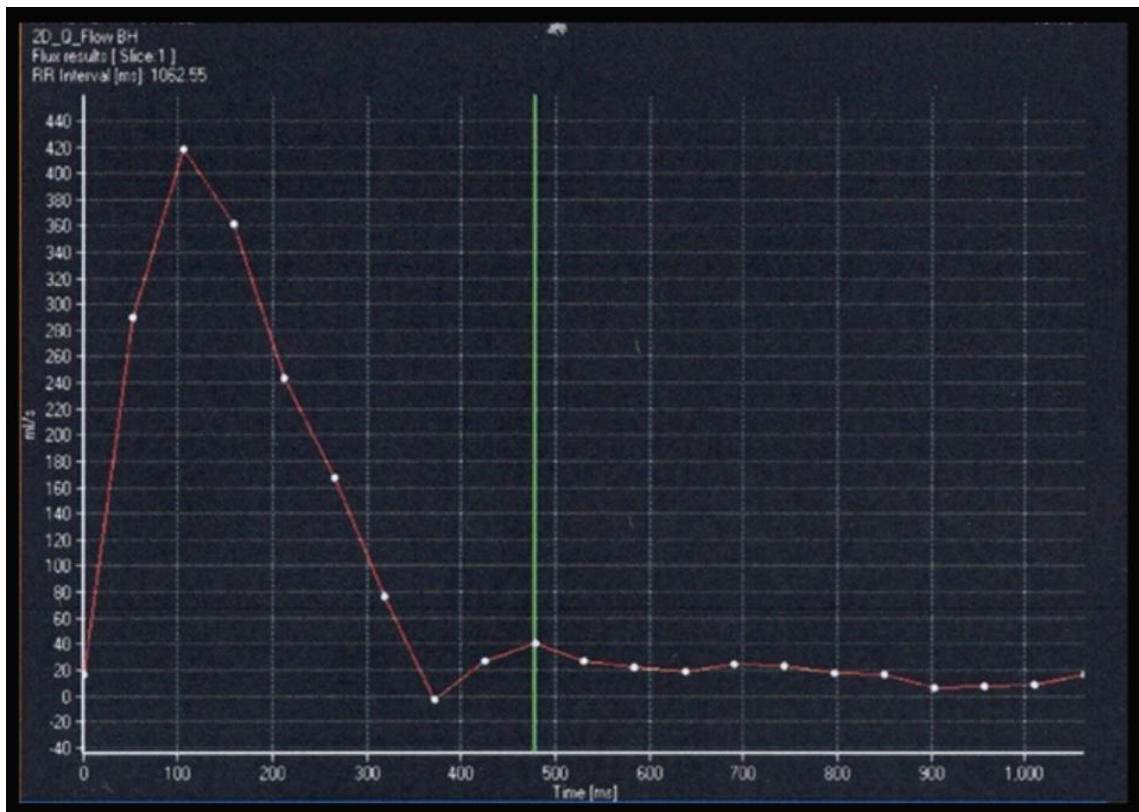


Figure 3.5. Time dependent volumetric flow rate on defined ROI

Other 3 of the data set are 3D phase-contrast MRI data, including characterization of time-resolved 3D blood flow velocities within a 3D volume data covering the entire aorta.

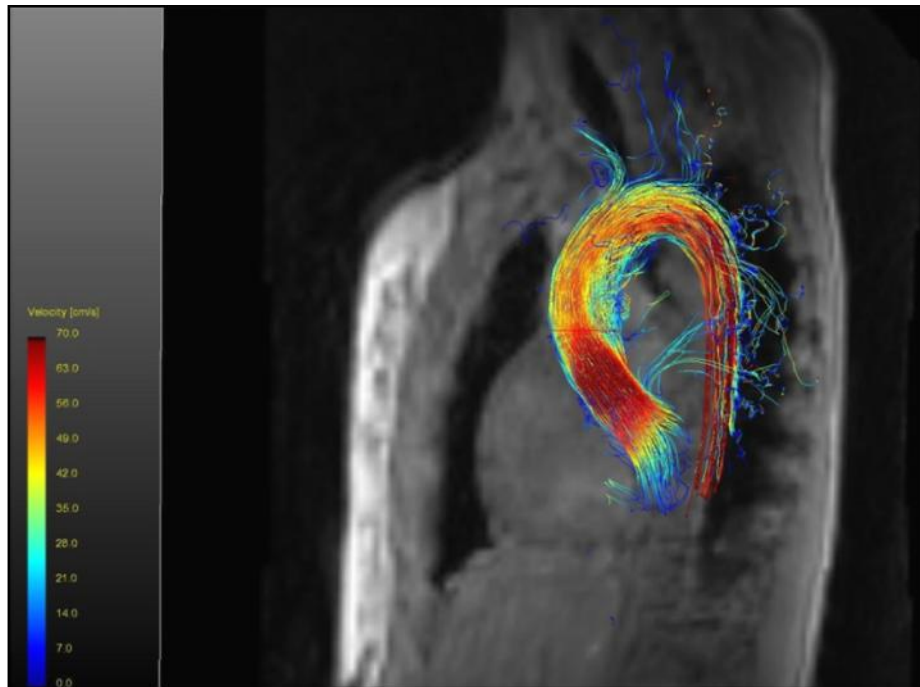


Figure 3.6. 3D time-resolved flow information through aorta

Phase contrast MR imaging has velocity encoding information possibility within the output images and this data was deciphered to produce velocity field maps for aorta flow, which is shown in Figure 3.6.

3.3. CAD GEOMETRIES

Aorta and left ventricle CAD geometries were reconstructed from patient-specific medical images. From 2-dimensional CT cross-section showing the geometry of the aorta combined and it was knit with the triangles. In Figure 3.7, a small triangle of cell surface was obtained as .stl file, which is a geometry file obtained from CT data by merging consecutive slices with the network structure.

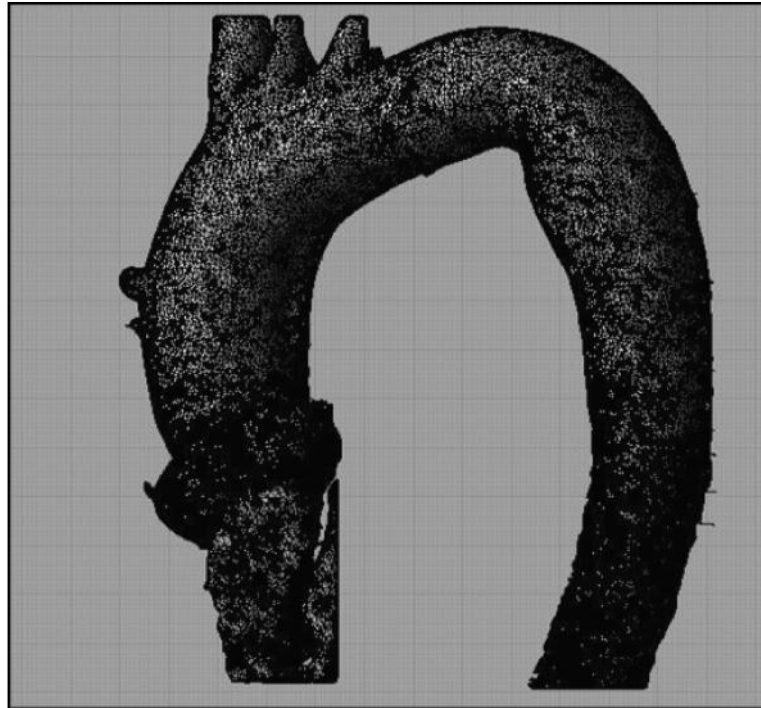


Figure 3.7. Aorta stl geometry

3.3.1. Aorta

CAD software called Rhinoceros was used to provide a link between surface networks that includes geometry information and 3D CAD model. The curves drawn from the point on the surface network so the geometry of the main lines has been identified. Combining the longitudinal and transverse networks created the limitations of the surface and then aorta geometry was obtained, which can be used in numerical analysis.

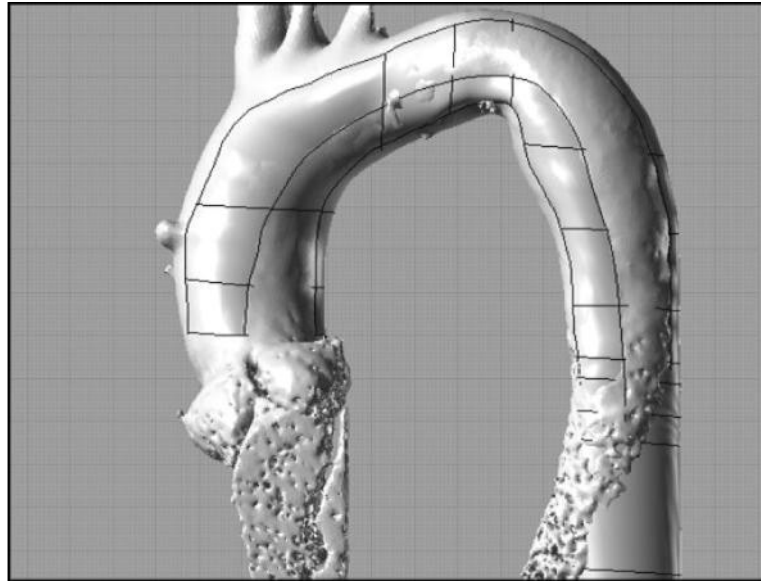


Figure 3.8. Aorta CAD geometry cross-section

3.3.2. Aorta-Artificial Artery Anastomosis

The conduit geometry was modeled as a tube with a diameter of 12 mm. In accordance with the purpose of study, examining the influence of the conduit position, some criteria were determined. Those are the location and the angle of artificial vessel. Thus, many combinations of different insertion locations and insertion angles were prepared.

Aorta-conduit connection locations of ascending aorta, descending aorta, and aortic arch were examined and the results of the numerical comparison studies are available [39, 21]. Clinical experience and literature based on the numerical results, artificial artery is connected to the ascending aorta is seen to be more appropriate. Connection will be made resulting in the ascending aorta, at the same location as the bypass link. 2 separate sections on ascending and descending aorta, perpendicular to the flow direction, the transversal plane were received. Mid-points of these sections together, determined the line progress of the blood from ascending aorta to the descending aorta on that transversal plane. This line was accepted as 90 ° line, and then conduit was placed to 90°, 100°, and 120° locations in Figure 3.9.

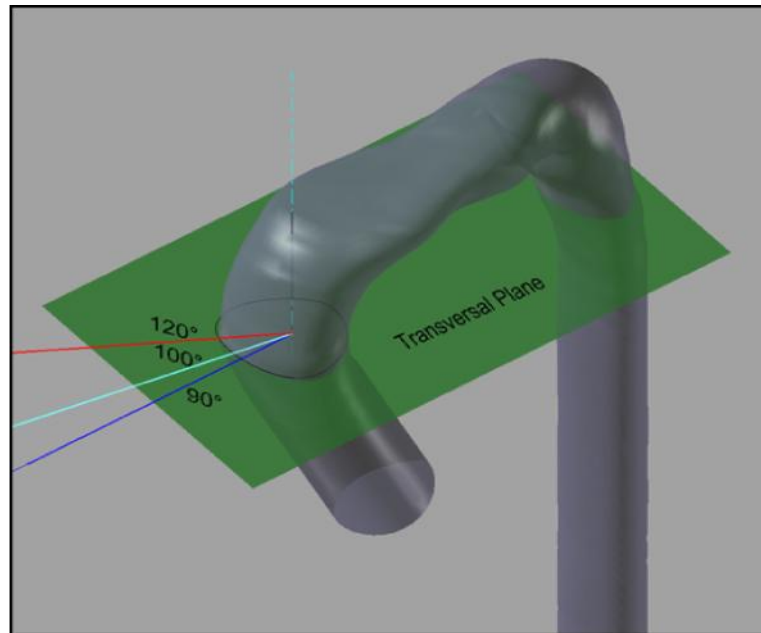


Figure 3.9. Conduit angle on the transversal plane

Another important criterion in aorta-conduit connection is the terms of the insertion angle of conduit. In the literature for artificial vascular connection such as 45° , 60° and 90° angles are used [40]. In clinical practice, however, the lower angle is preferred. In this study, 15° , 30° , 45° , 60° , 75° and 90° to 6 different angles for the geometry of the aorta-conduit anastomosis was drawn on the coronal plane. The coronal plane was defined from the line progress of the blood from ascending aorta to the descending aorta and axis of the ascending aorta, which is perpendicular to aortic valve. Therefore, 18 different aorta-conduit anastomosis geometries were prepared.

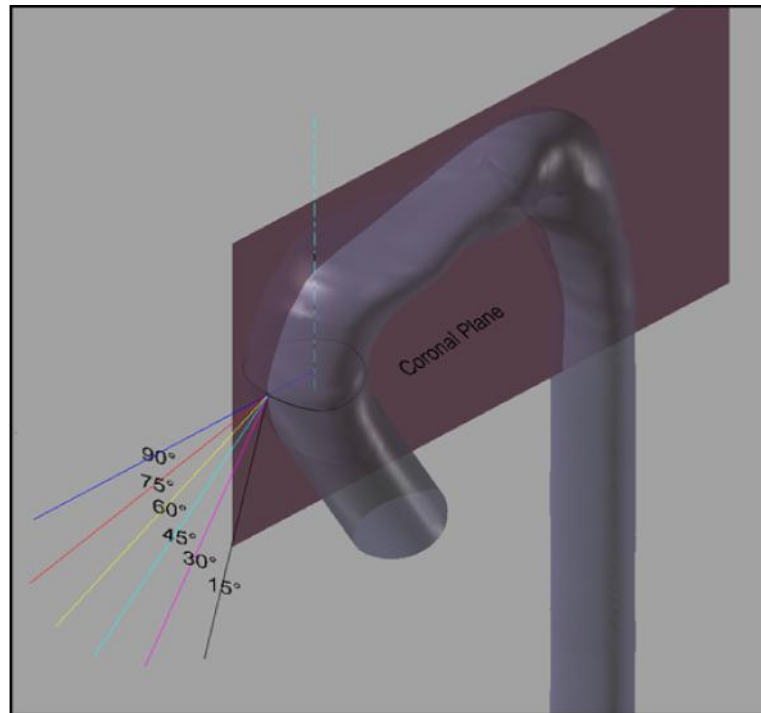


Figure 3.10. Conduit insertion angle on the coronal plane

The first designs were modeled by joining a rigid conduit geometry and aorta geometry. However, as the connection angle decreased from 90° to 45° degree, the anastomosis diameter increased rapidly, which is not acceptable in clinical applications, and moreover for the 30° and 15° designs the conduit geometry did not intersect the ascending aorta (see Figure 3.11, Figure 3.12 and Figure 3.13).

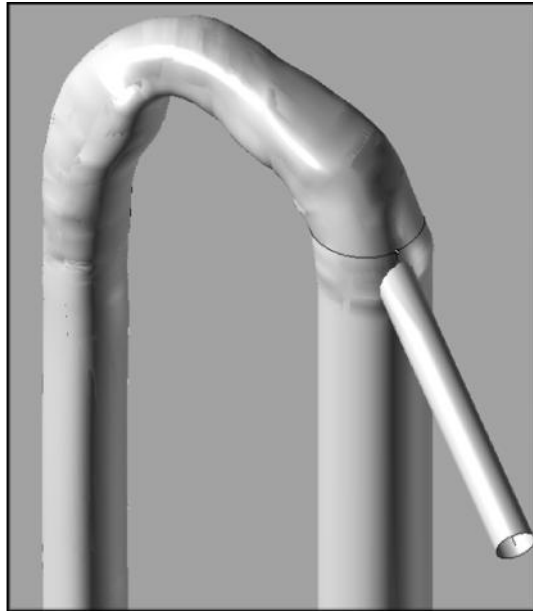


Figure 3.11. Artificial artery-aorta anastomosis design with 120° location angle and 60° connection angle

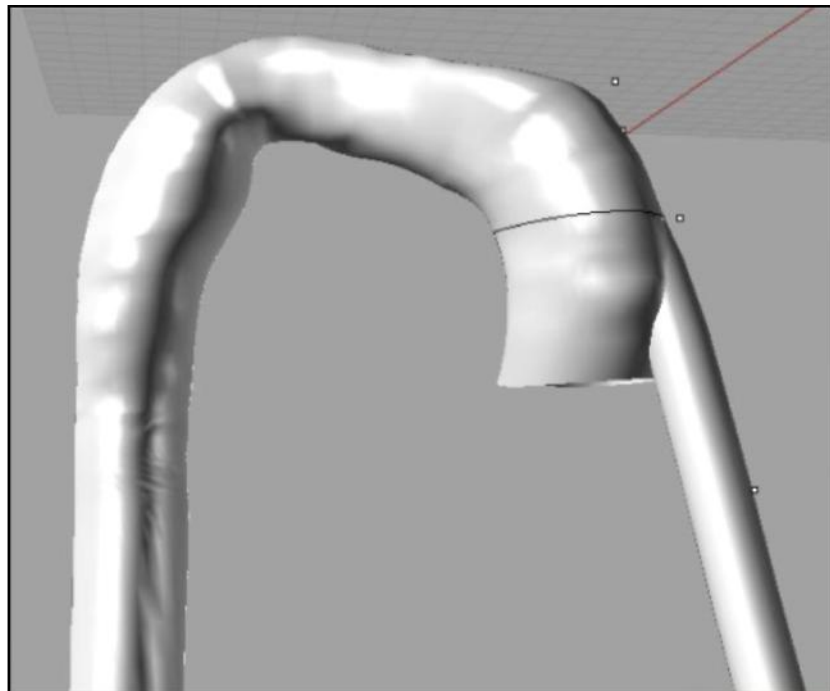


Figure 3.12. Artificial artery-aorta anastomosis design with 90° location angle and 30° connection angle

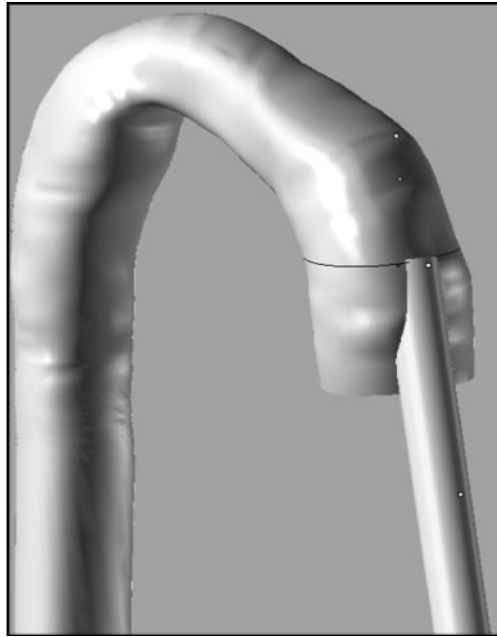


Figure 3.13. Artificial artery-aorta anastomosis design with 100° location angle and 15° connection angle

Therefore, new methodology was used to connect the artificial artery to the aorta and this time, the conduit geometry was modeled as having 90 mm length rigid part along the connection angle line, and near the connection it was curved to become perpendicular to aorta surface at connection point having 20 mm curved part showed in Figure 3.14.

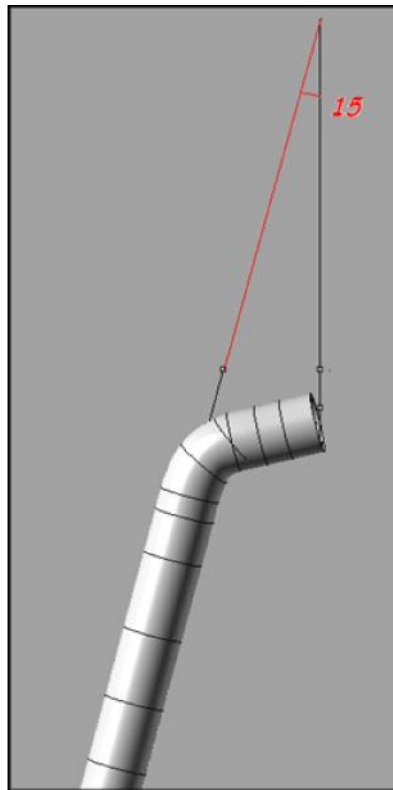


Figure 3.14. Design modification

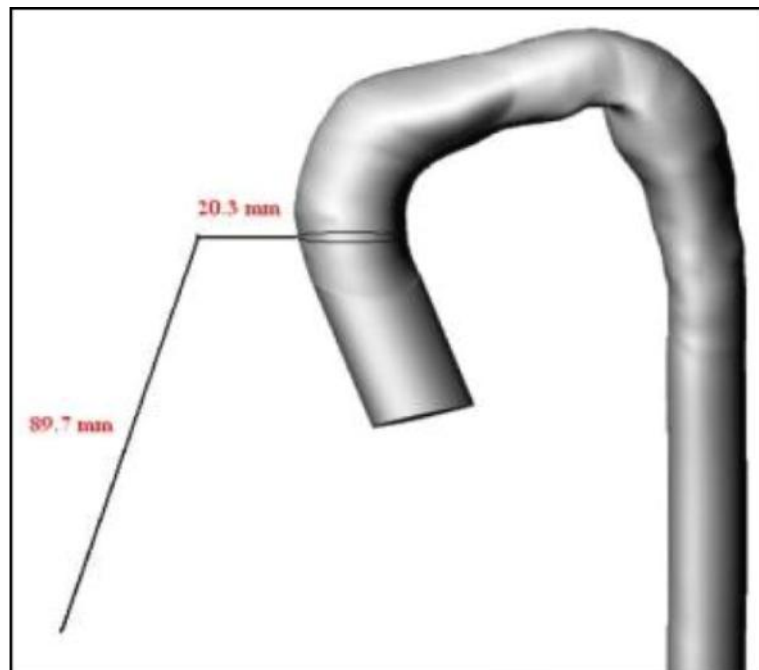


Figure 3.15. Artificial artery length

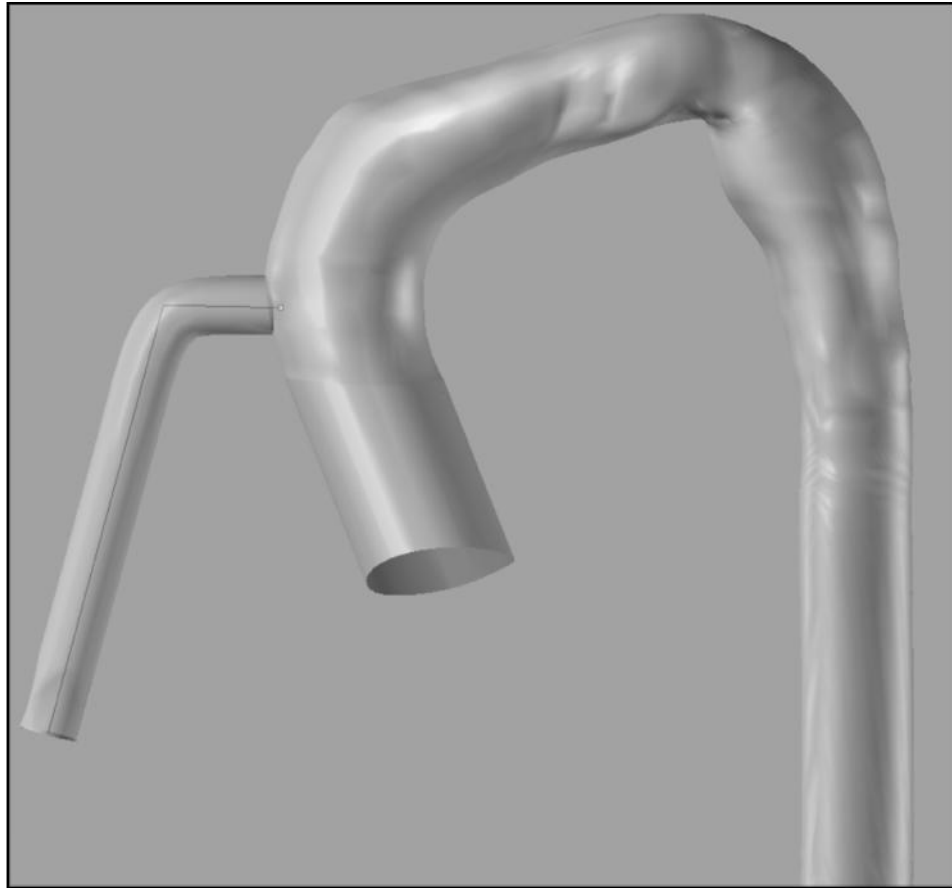


Figure 3.16. New artificial artery-aorta anastomosis design

For all 3 connection locations and 6 connection angles, the same procedure was applied, so both the rigid and curved parts of the conduit length and the joined angle of conduit surface and aorta surface were same for each 18 designs and showed in Figure 3.16.

3.3.3. Left Ventricle and Cannula

The reconstructed left ventricle geometry which was obtained from CT data had reduces eligibility for the CFD analysis according to the papillary muscles inside it. For this reason, to determine the geometry boundaries, from apex to aortic valves 5 mm distanced sections were taken perpendicular to apex of the left ventricle.

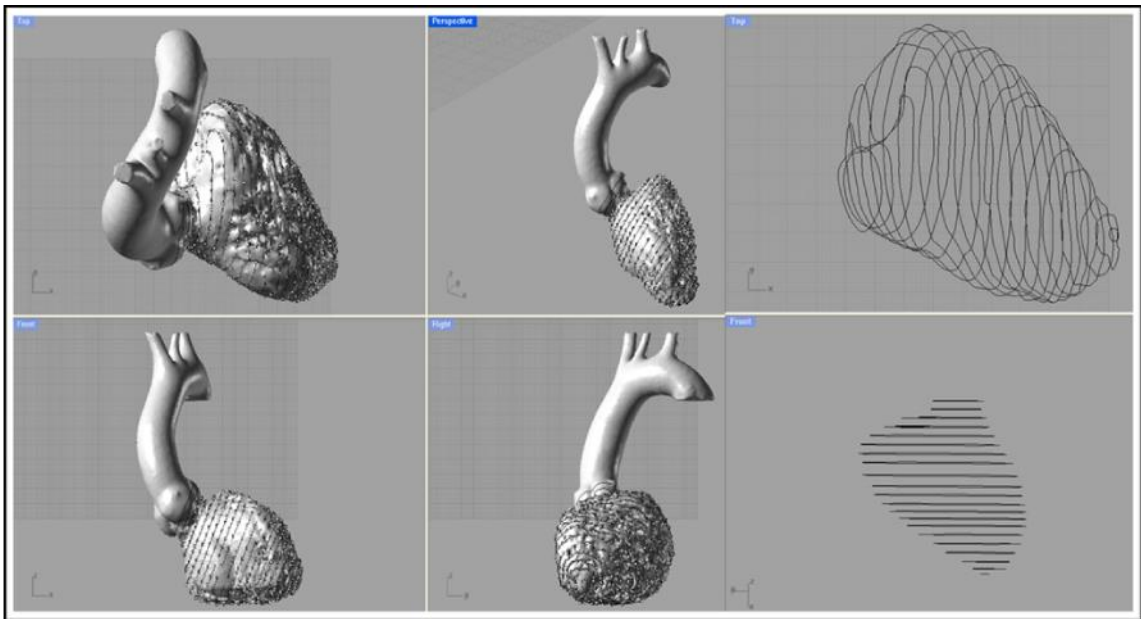


Figure 3.17. Left ventricle and aorta .stl file and left ventricle cross-section

Then appropriate left ventricle geometry was obtained by lofting a surface through these sections (Figure 3.18).

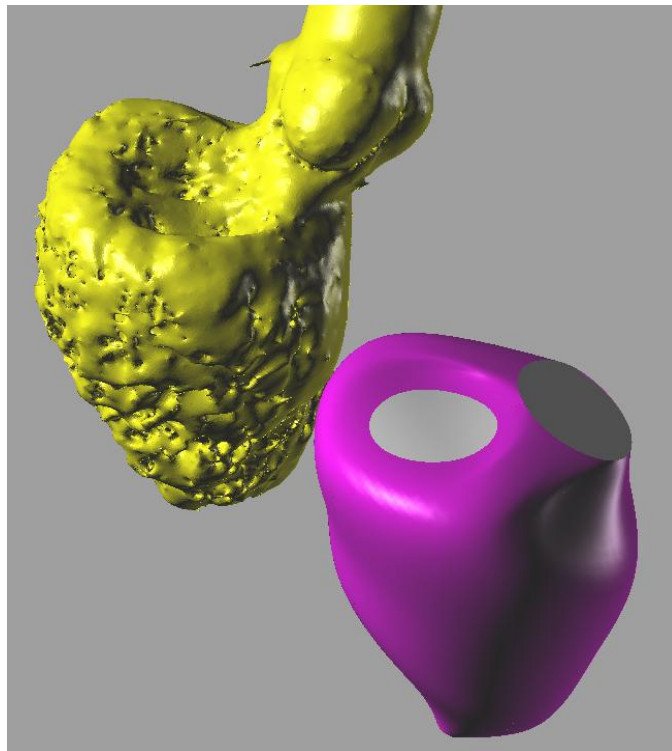


Figure 3.18. CAD design for left ventricle

Based on studies in the literature, the mitral and aortic valves were modeled as having fixed scale diameter and to prevent the flow field from non-physical boundary condition effects, the valves were extended up to 30 mm. Figure 3.19 shows the cannula geometry that was intersected with left ventricle geometry at apex, directing the middle of the left ventricle and its length was designed as about 53 mm.

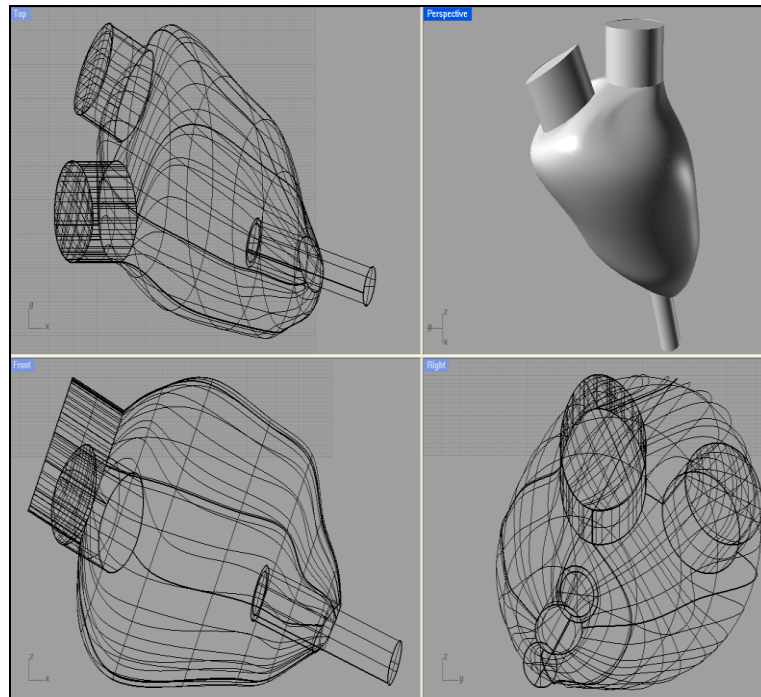


Figure 3.19. Left ventricle and cannula design

Heart failure patients with diseases of the heart's pumping ability of the blood from the left ventricle decreased slightly so the heart contractions were observed as decreased too. Therefore, for CFD analysis, the left ventricle geometry was modeled at constant volume.

4. FLOW INSIDE THE NATIVE AORTA

This study is largely focused on two major blood flow areas, namely, artificial artery-aorta anastomosis and left ventricle-cannula, to investigate the flow structure around the anastomosis location and cannula. However, as the biggest and strongest vein in human body is aorta to withstand against the blood leaving heart with high pressure and high velocity, the study was started by evaluating the aortic flow. Therefore, before the artificial artery-aorta connection, the steady and unsteady CFD simulations were performed with patient-specific aorta geometry alone, and the results were compared with the studies in the literature.

4.1. LITERATURE SURVEY

The uniform blood flow through the body is highly important for cardiovascular health. Any change in vein pathology and function will cause a non-uniform flow of blood, which can potentially lead to cardiovascular diseases. The examination of both vein anatomy and hemodynamics in vessel pathologies is of high interest for understanding, prediction and control of these diseases [41].

Even though one of the most difficult and challenging studies have been the researches of the hemodynamics with the complex anatomy of the vessels until today, the computational hemodynamics, which is the application of CFD to biological flow researches, provides a new level detailed information and successfully used to investigate the blood flow. Several CFD studies have been conducted on both idealized and patient specific geometries, to evaluate the blood flow characteristics, and present the relation between the cardiovascular diseases and cardiac vein anatomy and hemodynamics [42, 43].

4.2. GEOMETRY AND MESH

The inlet and outlet boundary of the aorta geometry, which was constructed from CT data, was extended to prevent non-uniform flow effects.

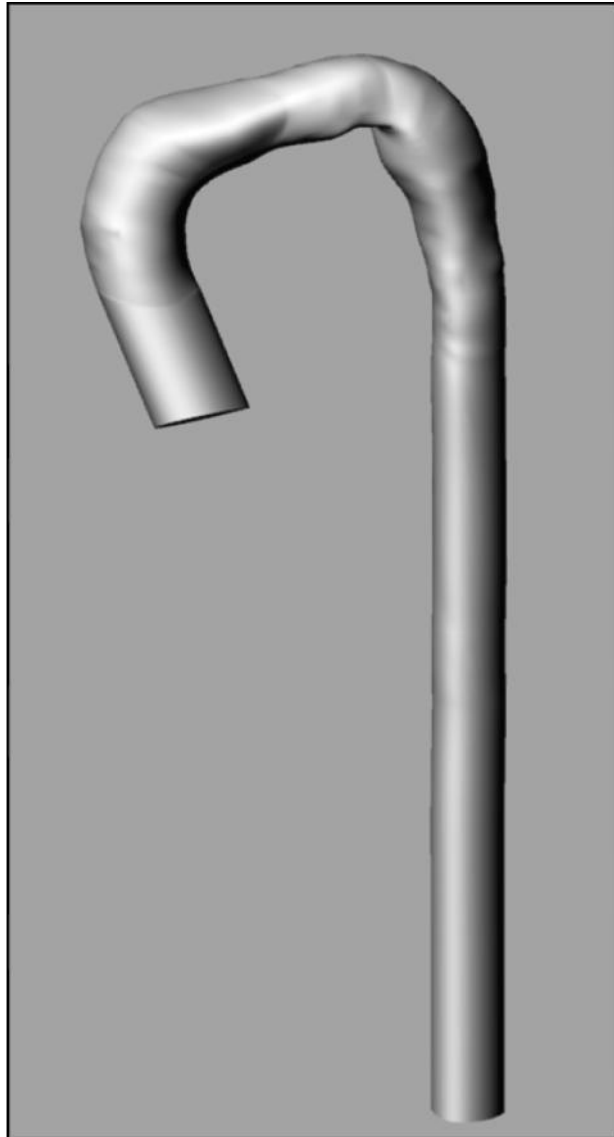


Figure 4.1. Aorta geometry that was used in CFD analysis

The calculated Re number only for aorta geometry was about 750, smaller than 2300, so the flow inside aorta was modeled as laminar. Also clinical researches give information about uniform flow inside aorta. However, the blood leaves the left atrium, and enters the aorta through aortic valves, has a pulsatile form according to the heart beats. So both steady and unsteady analyses were performed.

The mesh structure was defined according to the important part of the flow. For the flow only aorta geometry, the wall region, vessel arches are the important sections. So the mesh structure is very fine on the vessel wall, and it grows with a constant growth factor

from wall to the center. The distance from of the first cell from the wall was calculated with in two different ways, wall functions to get finer mesh resolution for laminar flow [44, 45] and Kolmogorov's scale.

An implication of Kolmogorov's (1941) theory of self similarity is that the large eddies of the flow are dependent on the geometry while the smaller scales more universal. This feature allows one to explicitly solve for the large eddies in a calculation and implicitly account for the small eddies by using a sub grid-scale model (SGS model). Thus, to solve most of eddies; the control volume needs very fine meshes. Consequently, very fine grids would eliminate the effect of the subgrid scale model and all the turbulent structures are completely resolved.

The meshes were done by using ANSY ICEMCFD program that enables to use block structure and the geometry was divided in O-grid block type.

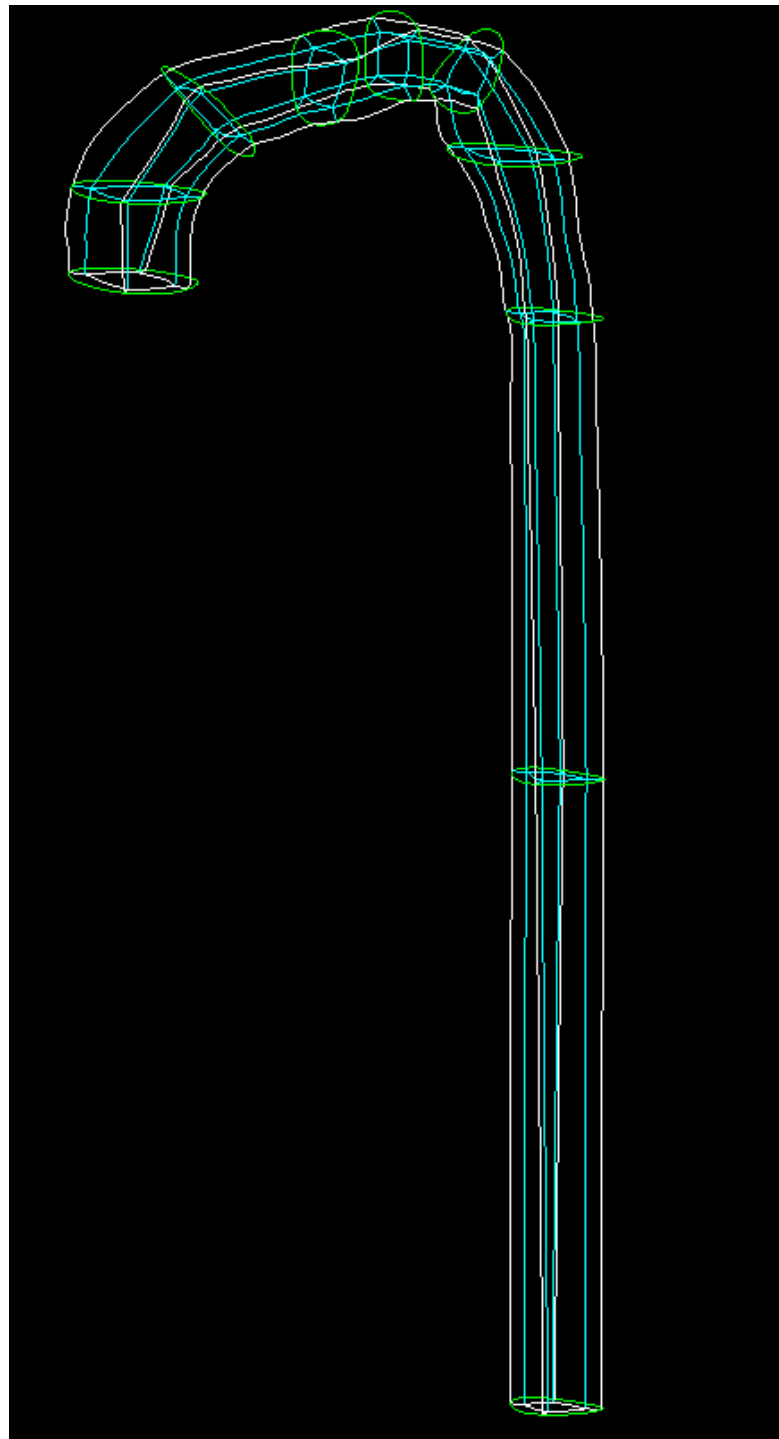


Figure 4.2. Block structure for O-grid type mesh

4.2.1. Law of Wall Functions

Table 4.1. Law of wall functions

THE TURBULANT BOUNDARY LAYER			
THE INNER REGION			THE OUTER REGION
THE LINEAR SUB-LAYER	THE BUFFER LAYER	THE LOG-LAW LAYER	Free from direct viscous effects.
Viscous stresses dominate. $u^+ = y^+$ $y^+ < 5$ Linear velocity profile	Viscous and Turbulent stresses are of similar magnitude. $5 < y^+ < 30$	Turbulent stresses dominate. $U^+ = 1/K^* (\ln y^+) + B$ $y^+ > 30$ Logarithmic velocity profile	

$$U^* = \sqrt{\frac{\tau_w}{\rho}} \quad (4.1)$$

$$C_f = \sqrt{\frac{\tau_w}{\frac{1}{2}\rho U_0^2}} \quad (4.2)$$

$$C_f = 2 \left(\frac{U_\tau}{U_0} \right)^2 \quad (4.3)$$

$$u^* = \sqrt{\frac{\tau_w}{\rho}} \quad (4.4)$$

$$y^+ = \frac{u^* y}{\nu} \quad (4.5)$$

Here the C_f value is taken from the literature calculation value as;

$$C_f = 0,027 * Re^{(-1/7)} = 0.0104$$

$$\tau_w = C_f * (0,5 * \rho * u^2) = 0.242$$

From equation 4.4 and equation 4.5 $u^* = 0.152$ and, for $y^+ = 1 \rightarrow y = 0.22$ mm here y^+ was chosen as 1, because for realistic analysis this value should be 1 or less than 1.

4.2.2. Kolmogorov's Scale

Kolmogorov microscales are the smallest scales in turbulent flow. They are defined by

$$\eta = \left(\frac{v^3}{\varepsilon} \right)^{1/4} \quad (4.6)$$

$$\tau_\eta = \left(\frac{v}{\varepsilon} \right)^{1/2} \quad (4.7)$$

Where ε is the average rate of energy dissipation per unit mass, and v is the kinematic viscosity of the fluid.

In his 1941 theory, A. N. Kolmogorov introduced the idea that the smallest scales of turbulence are universal (similar for every turbulent flow) and that they depend only on ε and v (46), then, $\eta = 0.32$ mm.

This value is the smallest scale in this flow. So in general, this value was fixed inside the boundary. But for the meshes near the wall, the previous value was used as 0.22. Because, the eddies are really became very small near the wall, because of the no-slip boundary conditions.

4.3. MESH INDEPENDENCY

To find the appropriate number of control volumes for aorta CFD simulations, mesh independency test was performed. Therefore, for the same aorta geometry 4 different cases were prepared, where the distance of the first cell from the wall, growth rate were same, only the total number of control volumes increased uniformly (Figure 4.3).

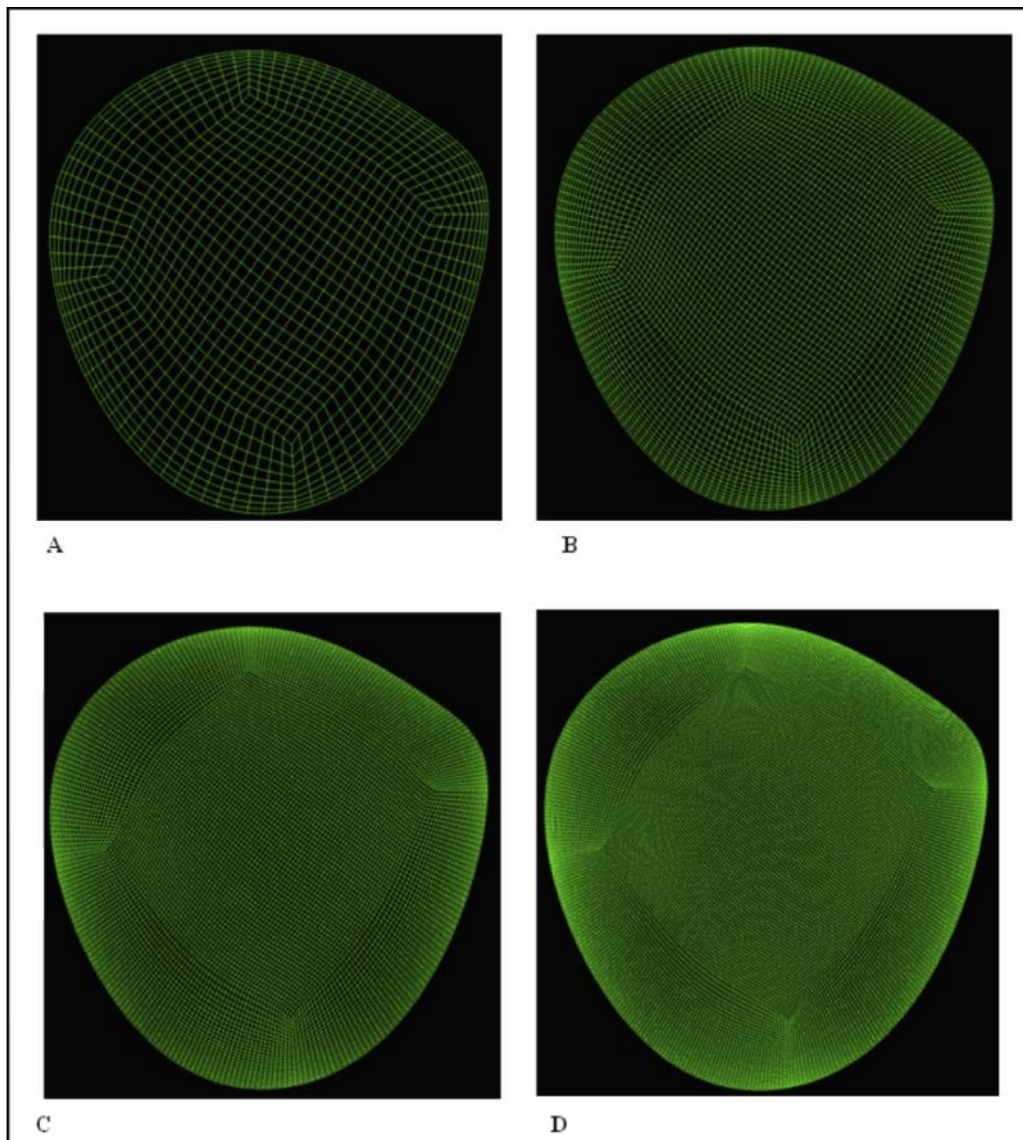


Figure 4.3. Different number of control volumes for 4 test cases; A) 72000, B) 550000, C) 2000000, and D) 5000000

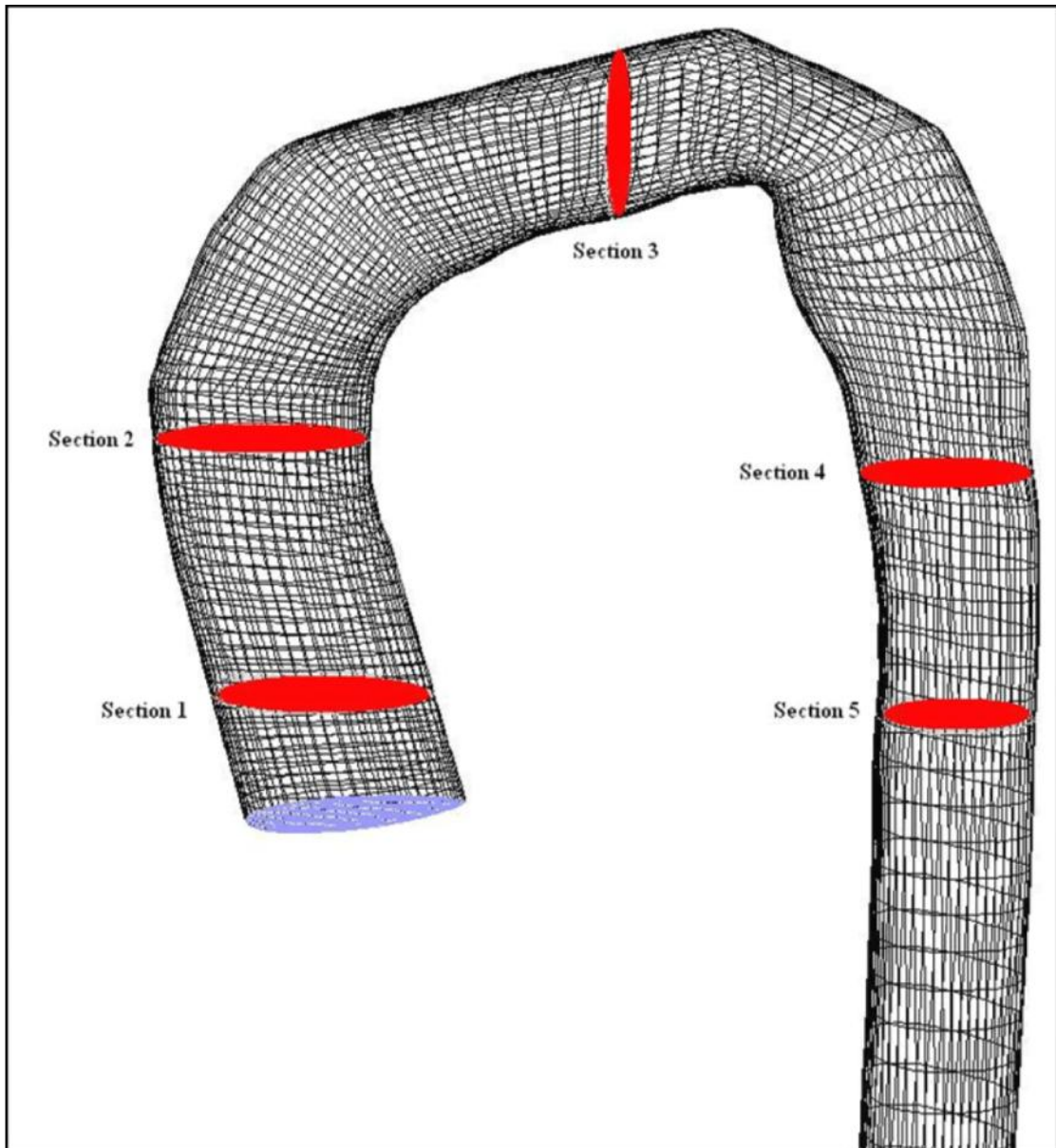


Figure 4.4. Velocity sections

For each three cases, with the same boundary conditions, solution methodology and converging criteria values, laminar and steady CFD analysis were performed. The results were evaluated considering, pressure change, pressure distribution on the middle section and velocity vectors on the sections.

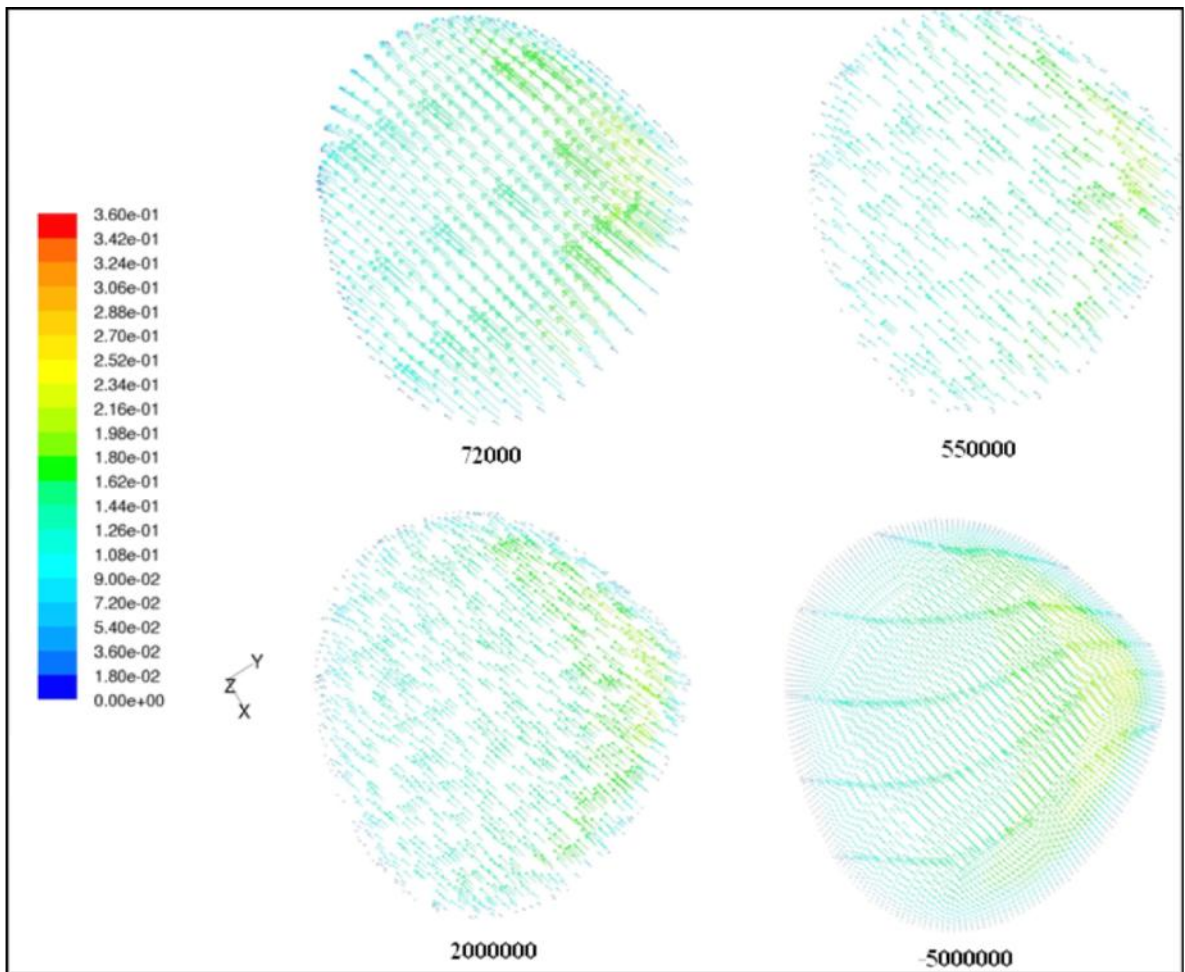


Figure 4.5. Velocity vectors on the section-1

The higher resolutions for secondary flows were succeeded with the increased number of control volumes are shown in Figure 4.5.

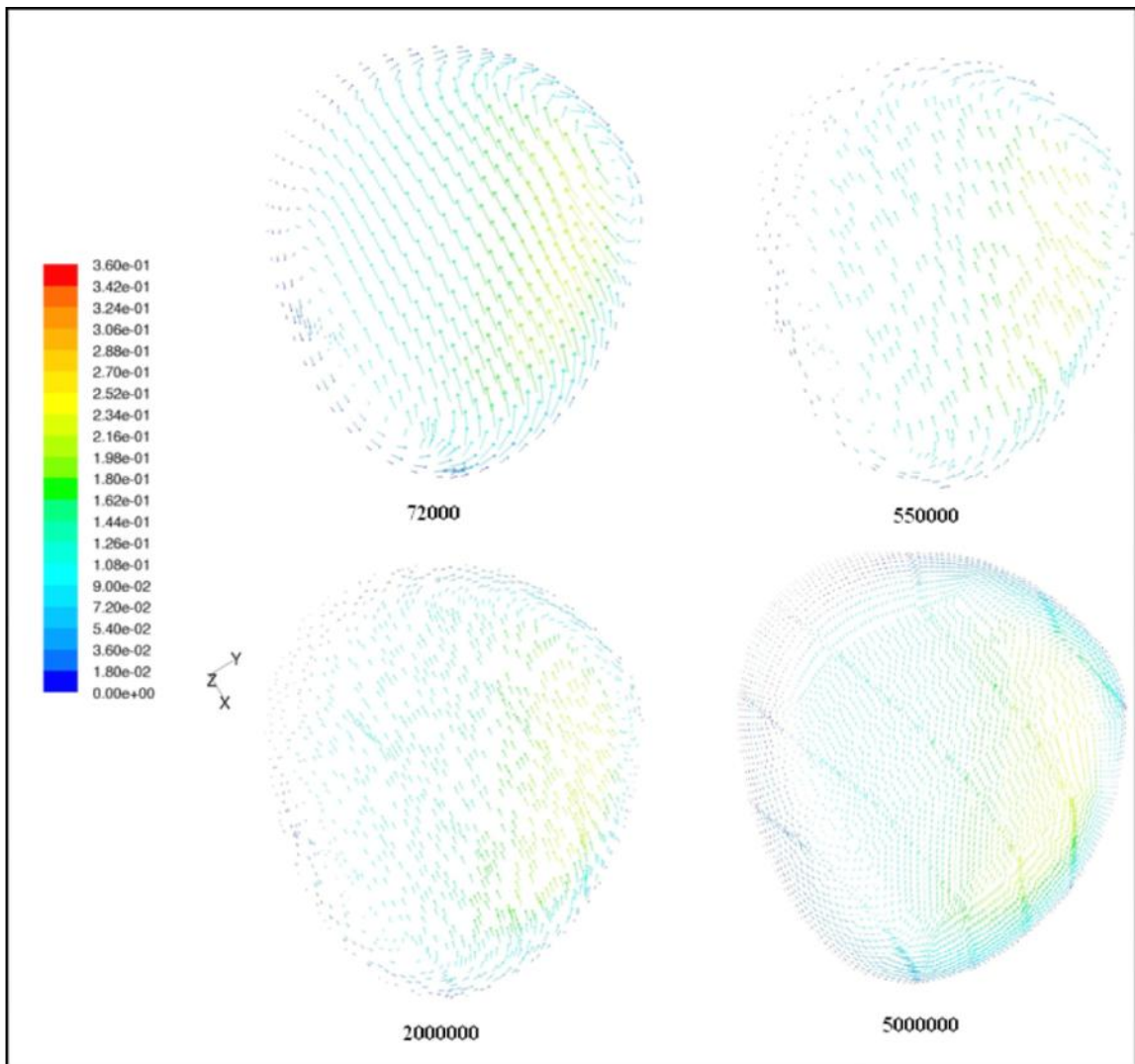


Figure 4.6. Velocity vectors on the section-2

The second section is taken on the ascending aorta, the secondary flows are seemed near the vein wall and similar to the previous representation, the more number of control volumes, the higher resolution is gained that are shown in Figure 4.6.

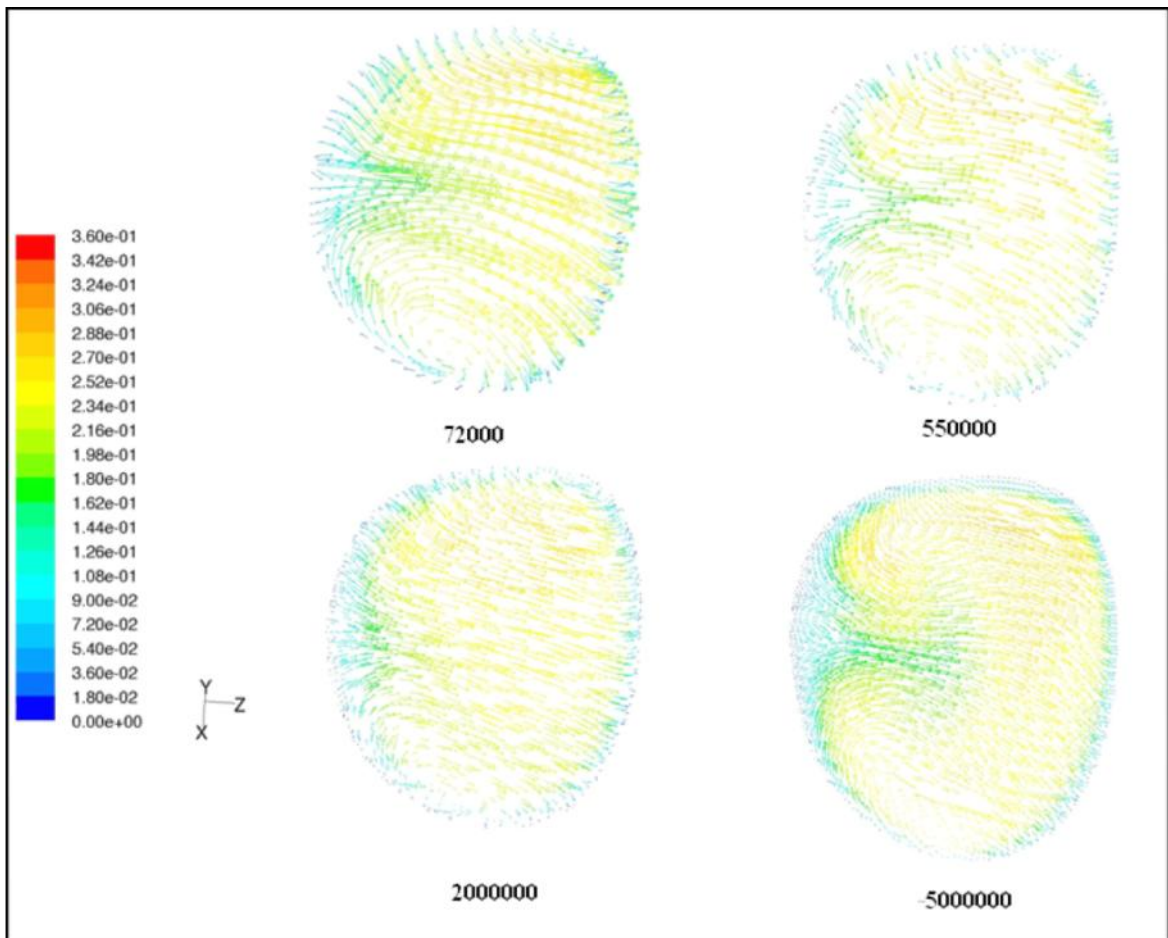


Figure 4.7. Velocity vectors on section-3

For third and fourth cases, the results are seemed to each other so this can be concluded as after 2 million control volume the simulations become independent from the number of control volumes.

4.4. CFD ANALYSIS

The CFD simulations were performed by using a commercial code named Fluent, based on a control-volume based technique. The fluid equations were solved with segregated pressure based implicit method, and all pressure and momentum equations were discretized with 1st order upwind model. The convergence criteria were set to 10^{-3} for residuals. The fluid was modeled as blood, and regarded as homogeneous Newtonian fluid having density of $\rho=1050 \text{ kg/m}^3$ and viscosity of $\mu=0.0035 \text{ kg/m-s}$. According to the Re number, the flow inside aorta was modeled as laminar flow [47]. The wall boundary

condition and the aorta outlet boundary conditions were set as no-slip boundary condition and pressure outlet respectively.

4.4.1. Steady, Constant Mass Flow rate

The first CFD simulations were performed steady and constant mass flow rate of 6lt/min.

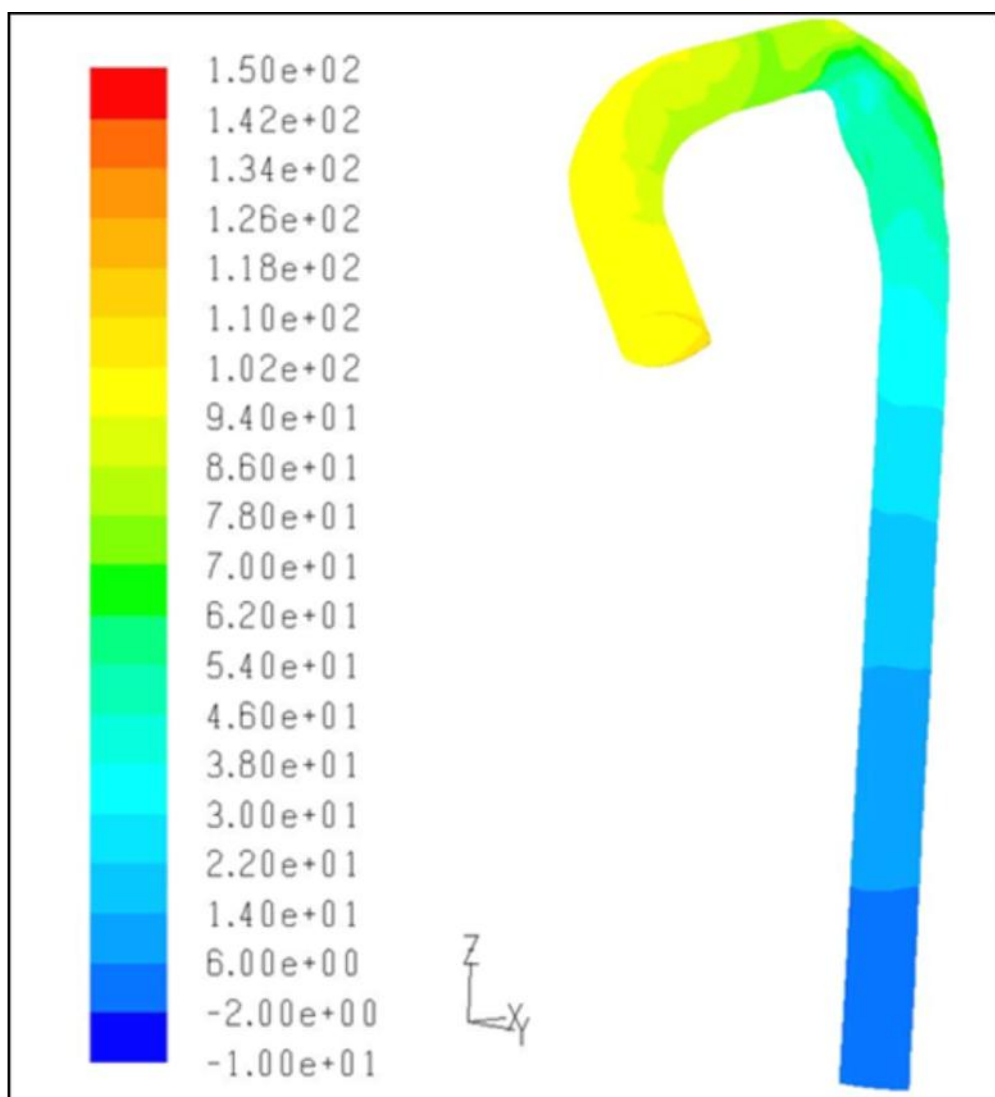


Figure 4.8. Pressure distribution on aorta wall

The pressure distribution on the aorta wall is seemed to decrease from ascending aorta to descending aorta uniformly. However at the descending aorta arch, the reverse flows cause rapid changes on the pressure distribution.

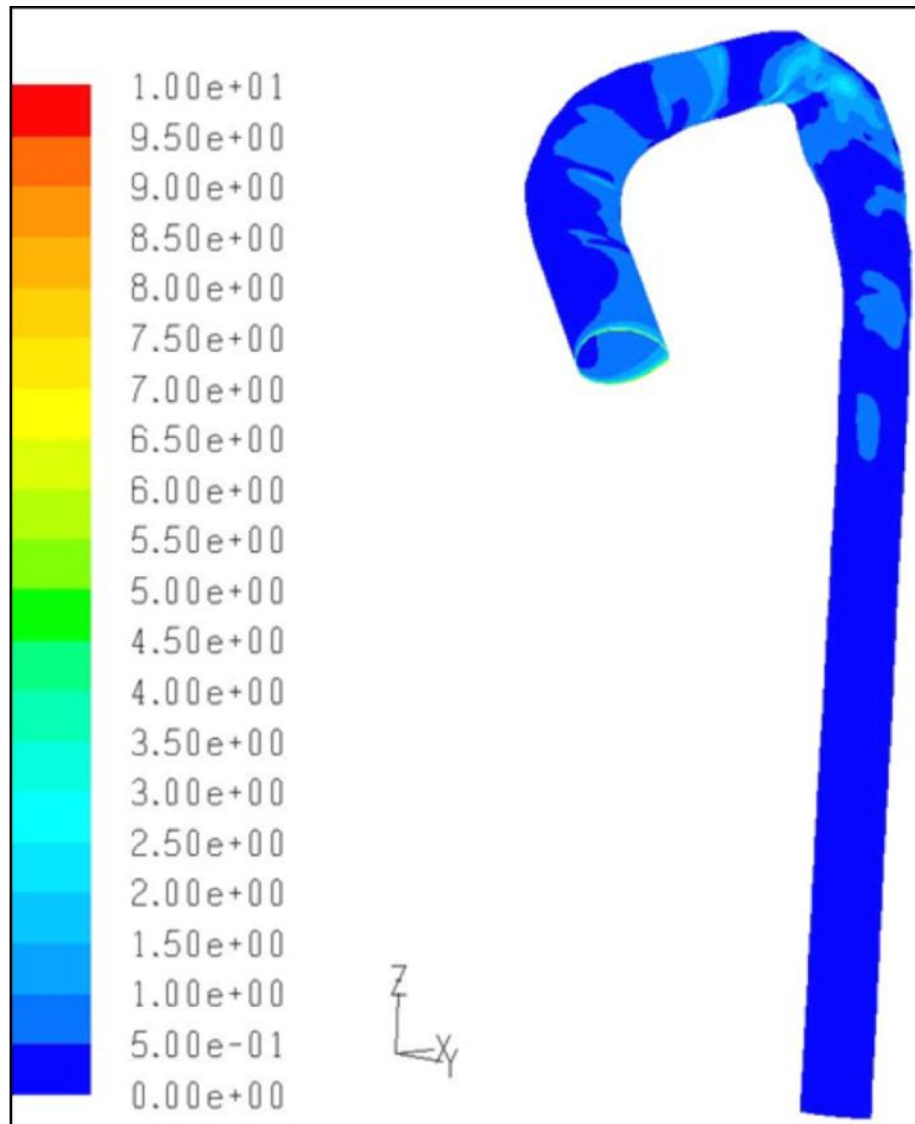


Figure 4.9. WSS distribution on aorta wall

The wall shear stress (WSS) distribution on the aorta wall is high at ascending aorta, where just above the aortic valves and aortic arch, where the pressure and velocity values change according to the changing geometry. Any change on the velocity structure lead to a change on pressure and WSS distribution.

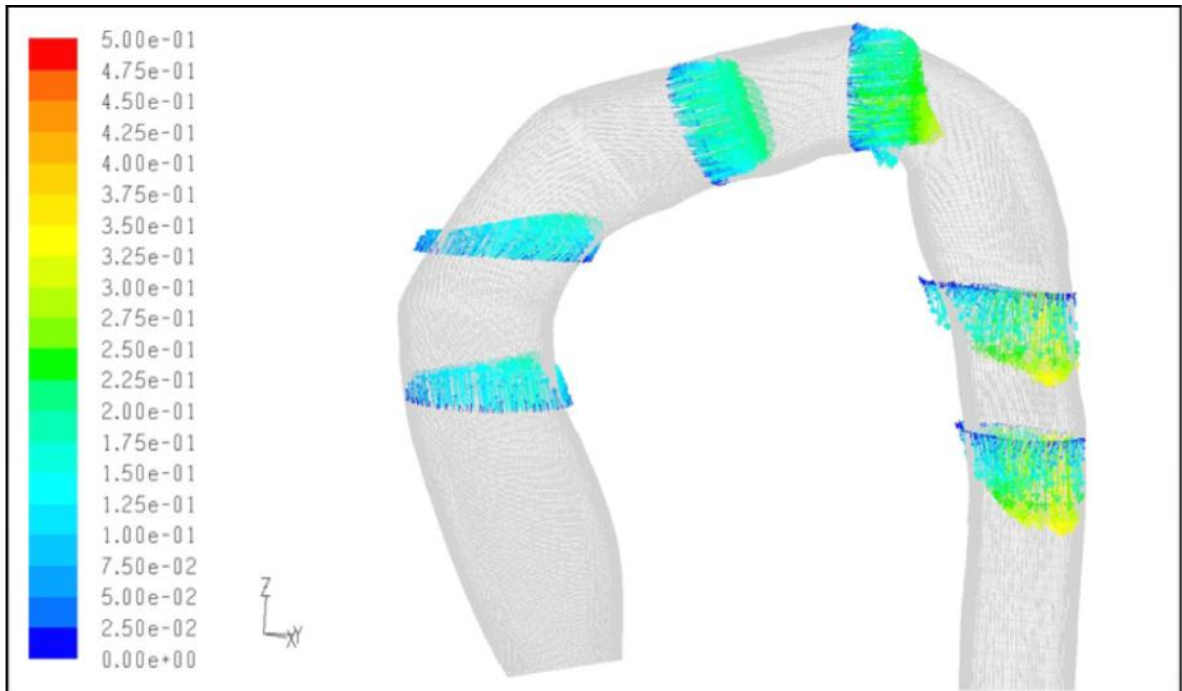


Figure 4.10. Velocity vectors through aorta

From ascending aorta to descending aorta, some sections were taken perpendicular to the flow direction and velocity vectors are examined. The velocity values are 0 on the wall due to the no-slip boundary condition, and their values increase towards the vein center.

4.4.2. Unsteady, Pulsatile Mass Flow rate

The time dependent, pulsatile flow simulations were performed after the steady CFD simulations. The inflow boundary condition was defined from MRI data (Figure 3.5). The realistic waveform of blood flow was divided into three parts to reduce the degree of the MATLAB function. The first part, the difference between 0 ms and 478 ms was formulated with fourth degree of Lagrange interpolation equation, the second part of the change between 478 ms and 744 ms was formulated with third degree of Lagrange interpolation equation and the third part was modeled as constant [48, 49].

$$\begin{aligned}
 p(x) = & \frac{(x-x_1)(x-x_2)\dots(x-x_n)}{(x-x_1)f'(x_1)}y_1 + \frac{(x-x_1)(x-x_2)\dots(x-x_n)}{(x-x_2)f'(x_2)}y_2 \\
 & + \dots + \frac{(x-x_1)(x-x_2)\dots(x-x_n)}{(x-x_n)f'(x_n)}y_n
 \end{aligned}
 \tag{4.1}$$

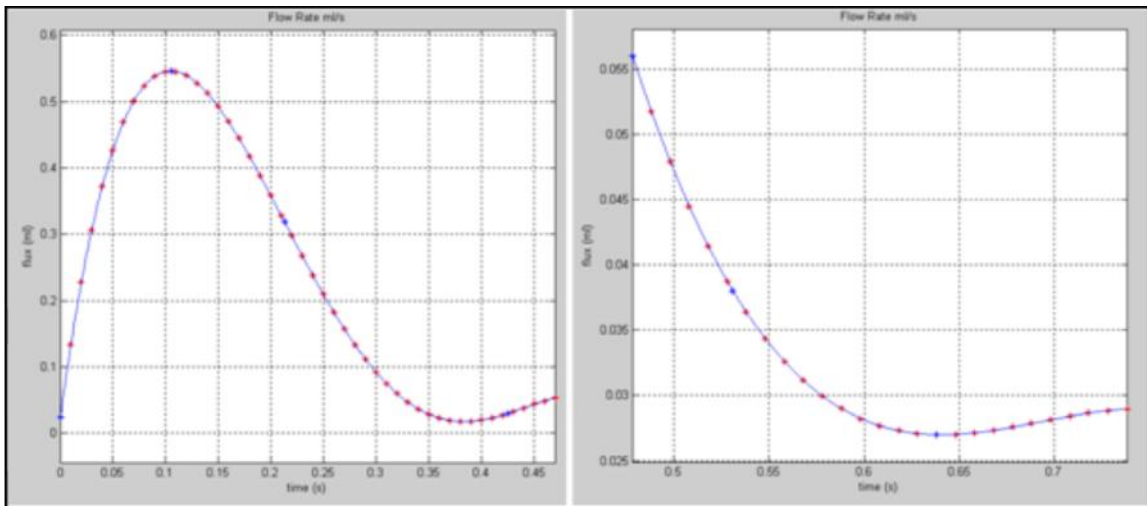


Figure 4.11. Lagrange interpolation equations graph

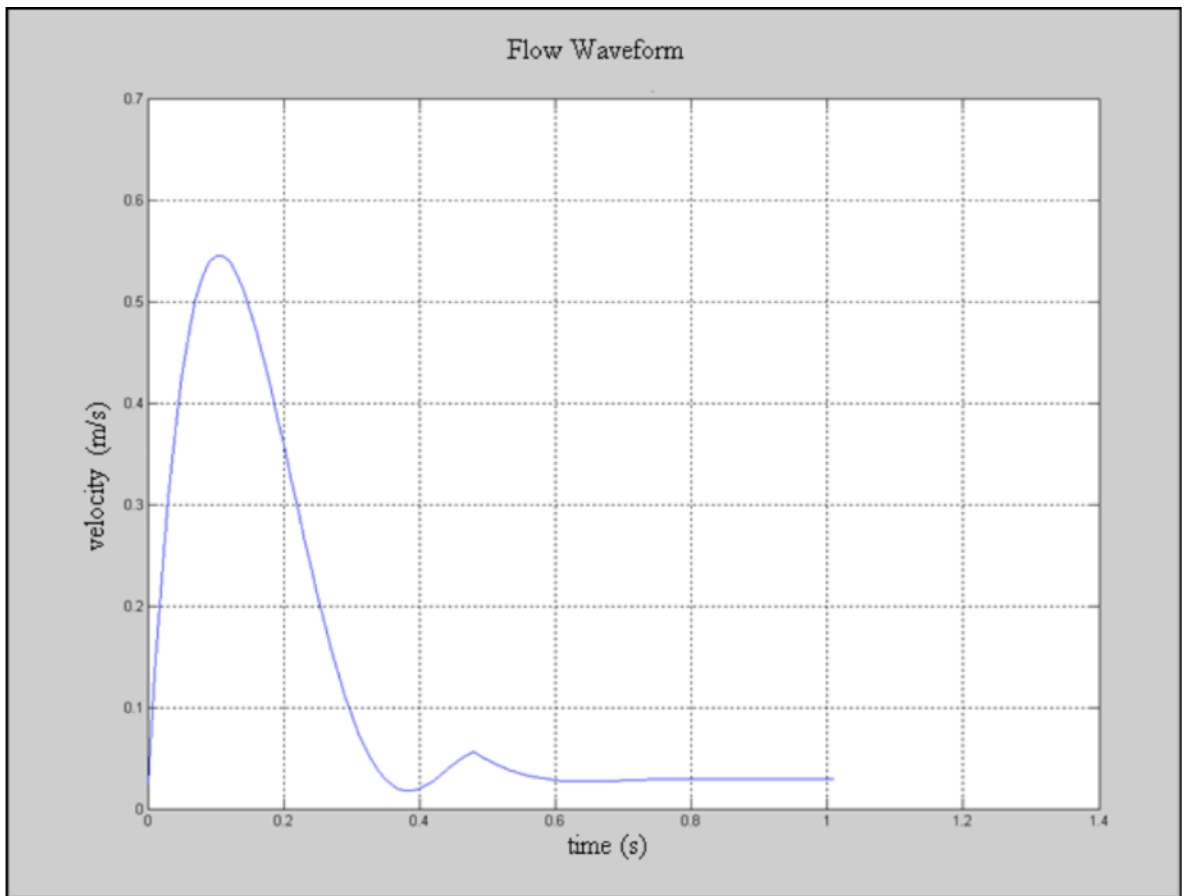


Figure 4.12. Pulsatile flow waveform derived from MATLAB code for Lagrange interpolation equation

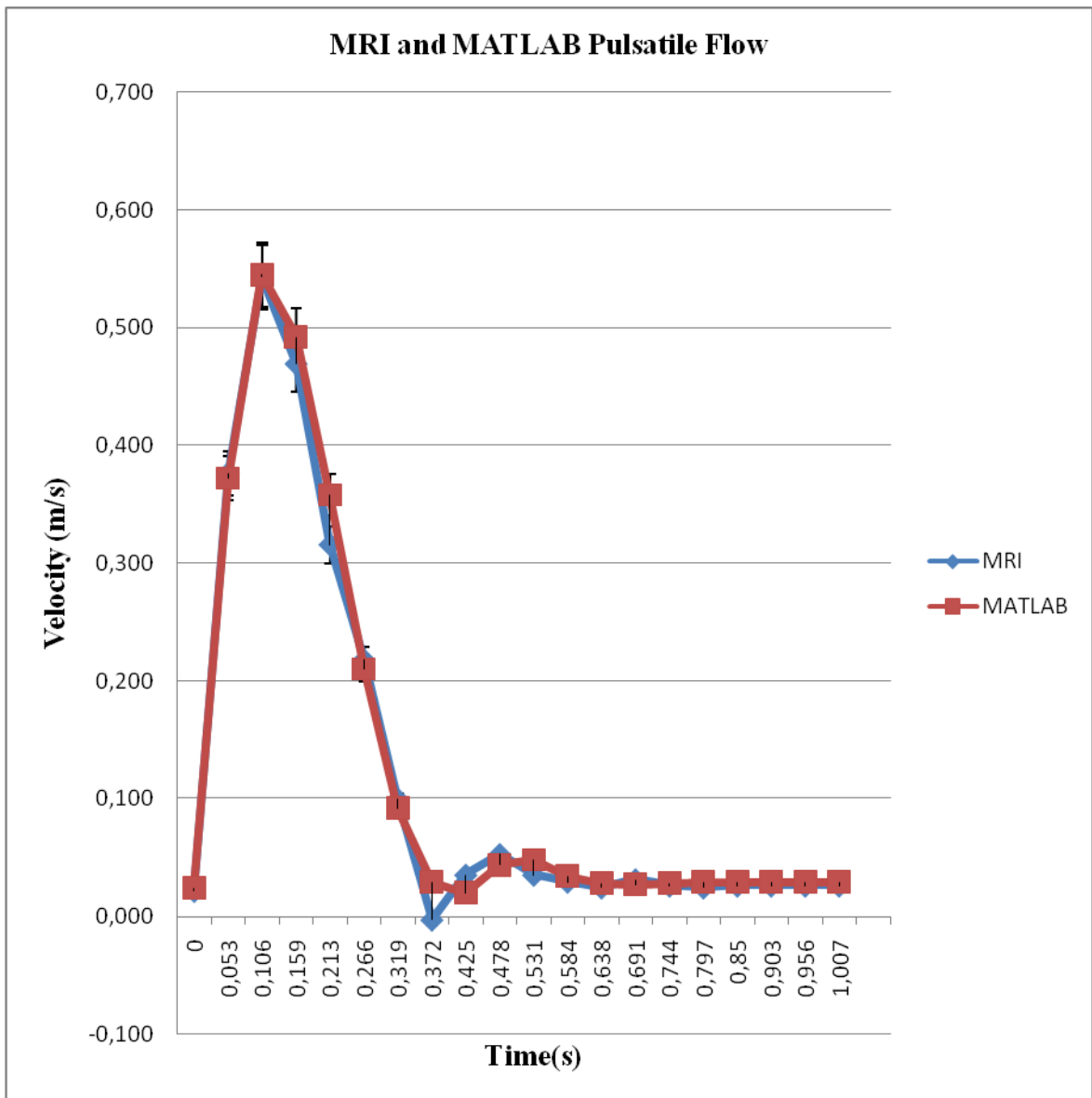


Figure 4.13. MRI and MATLAB flow waveform

The calculated values using Lagrange interpolation equations are similar to the real MRI values; thereby the error bar values are very small (Figure 4.13). To eliminate the negative flow effects seem at 0.378 s, the whole values were shifted. The realistic flow profile equated with MATLAB code was set into FLUENT using user definition function (UDF) for inflow boundary condition at aorta inlet.

The patient's heart beat was measured as 60 beats/min, and each heart beat was divided into 20 phase within 53 ms, so the period became $T=1.007$. For unsteady CFD

simulations, to investigate the time dependent flow accurately, the time step size was calculated as 1/10 of beating phase and period was divided into 190 steps. Therefore, the time step size was 0.0053 and to evaluate 5 heart beatings, 950 number of time steps were used.

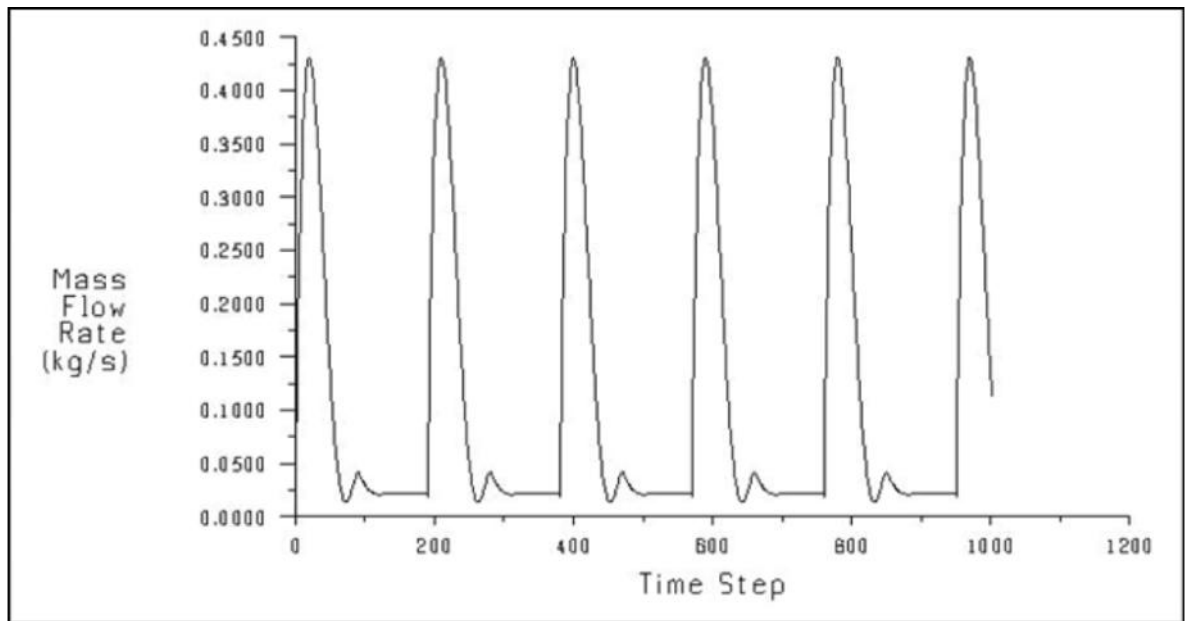


Figure 4.14. Time dependent pulsatile mass flow rate graph from FLUENT simulation

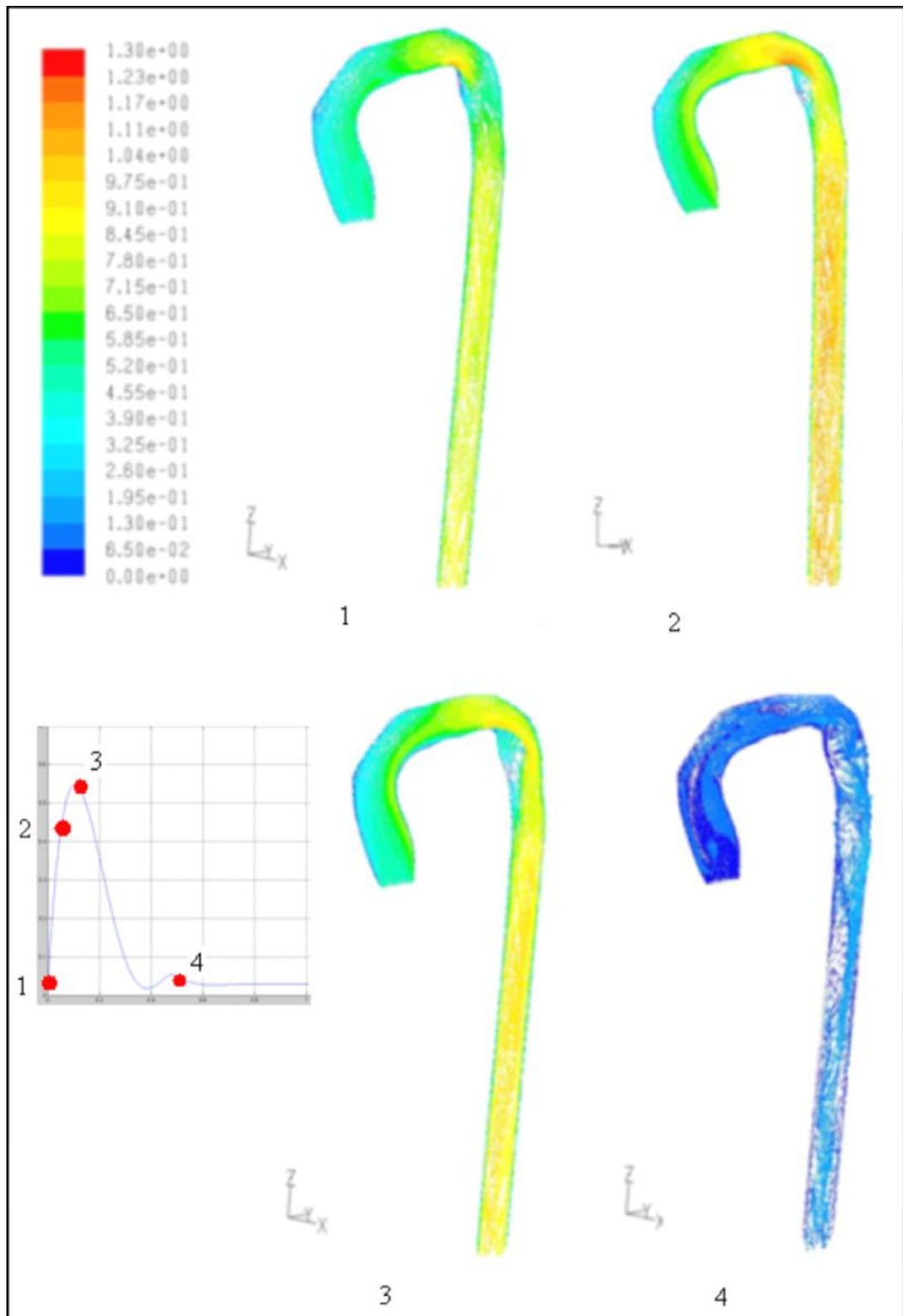


Figure 4.15. Velocity vectors (m/s) of time dependent unsteady CFD simulation

4.5. CONCLUSION

Before the investigation of the hemodynamics within the aorta-artificial artery anastomosis model flow, to earn a knowledge about flow structure inside aorta, both steady and unsteady CFD analysis were performed using patient-specific aorta geometry. The results reported here, focusing on i) velocity profile, ii) pressure distribution and iii) wss distribution.

The steady analysis was performed with constant mass flow rate at aorta inlet, and mapping of the velocity components allowed comparison of flows in different studies. The flow profile through ascending and descending aorta is similar to other studies, however due to the geometrical changes through the aortic arch some recirculation occurs at the ascending and descending arch, which in result; link the relation between the vein anatomy and flow patterns properties.

The realistic unsteady CFD simulation was performed with real inflow boundary conditions and the obtained velocity patterns were quantitatively compared to velocity patterns obtained from 3D MRI. In Figure 4.15 and Figure 4.16, even though the patient specific model of the CFD simulation was different from the MRI model, the flow structure shows similarities considering time-dependent flow information.

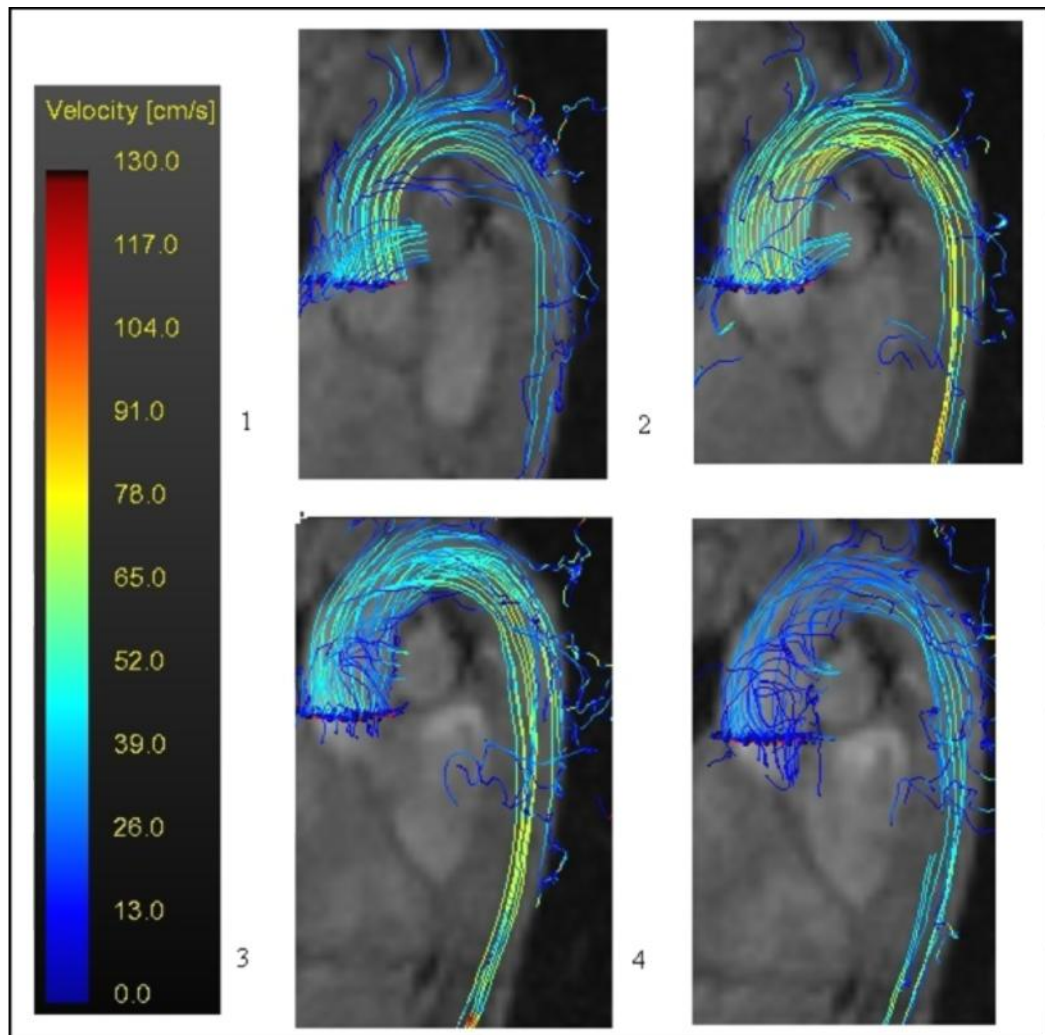


Figure 4.16. MRI flow patterns

5. AORTA-ARTIFICIAL ARTERY ANASTOMOSIS

Left ventricular assist devices are mechanical pump-type devices that are used for improving the function of the failing left heart. The inflow conduit of the LVAD, which is connected to the apex of left ventricle, pulls blood from the left ventricle into a pump, while the outflow conduit is connected to the aorta to enable the oxygen-rich blood circulation throughout the body. Flow in the aorta is highly affected from the aorta-conduit anastomosis structure, i.e. any change in the hemodynamic through the aorta-conduit anastomosis causes deformation of blood cells and endothelium [50]. Therefore, to decrease these important effects, CFD analysis were performed with 18 different anastomosis designs, and the results were compared in terms of velocity profiles, pressure and wall shear stress distribution.

5.1. LITERATURE SURVEY

There have been important developments in many aspects of LVADs, such as reducing the weight, increasing the battery life and enabling the device control, which in turn increase the implantation rates [33]. Nevertheless, after LVAD implementations, some potentially fatal and ruinous complications remain, including infections and device failures [51]. Even with optimized devices, some other lethal complications can occur due to the deformations through the aorta-conduit anastomosis.

In order to increase the performance of LVADs as well as to anticipate complications that could occur, a myriad of studies have been done. Many studies, however, only pertain to the blood flow in heart pumps [19, 20, 21]. Yet, due to the high rotational speeds of pumps, blood cells pass through the pump rapidly and without undergoing any deformation. Therefore, it is important to study the flow inside the aorta, which is seriously affected in terms of aorta-conduit geometry.

The effects of the insertion angle and the location of the conduit have been investigated by May-Newman *et al* in two separate studies that steady flow develops both

in series and in parallel. In the first study, CFD simulations were done to investigate the effect of surgical anastomosis configuration of the aortic outflow conduit on the flow fields in the aorta. 2 cylindrical tubes that intersect at angles ranging from 30° to 90° were used [40]. In the second study, curved tube model was used for aorta geometry and the conduit geometry was placed on 3 different location on the aorta model, to investigate the effect of LVAD aortic outflow conduit location [39]. Tokuda *et al* did a similar study during cardiopulmonary bypass. The steady blood flow in the aortic arch was simulated to get information on the flow details [52]. Biswajit Kar *et al* studied the effects of outflow-graft anastomosis location on flow in the thoracic aorta, performing 2- dimensional numerical simulations of flow in an aortic model. The cylindrical channel that represents outflow graft was attached to either ascending or descending aortic location of the curved model [53]. Litwak *et al* have a different approach to this issue in terms of studying the effects of continuous flow (CFVAD) and pulsatile (PVAD) ventricular assist devices on the aortic blood flow as a measure of overall blood distribution in an acute calf model [21]. Bazilevs *et al* studied the unsteady-pulsatile flow in the patient-specific model of the aorta with an added LVAD outflow conduit in the descending portion of the aorta. The combined model was considered under three different flow conditions as LVAD was closed, LVAD was operating half, and LVAD was operating fully [54].

In general, the clinical success means to reduce the flow abnormalities and to obtain uniform flow fields at the inlet and at the outlet of the pump as well as the flow through the pump around the anastomosis.

5.2. GEOMETRY AND MESH

The mesh structure was defined according to the important part of the flow. In this study, different from the aorta only simulations, the wall region, vessel arches and the anastomosis location are the important sections. So the mesh structure is very fine on the vessel wall, and it grows with a constant growth factor from wall to the center. The distance of the first cell from the wall was calculated by Kolmogorov's scale as 0.02mm.

For each 18 anastomosis design, about 4.3 million same control volumes with the structure were prepared using the commercial software named Ansys IcemCFD.

5.3. TURBULENCE MODELLING TEST

To find the appropriate turbulence models, 5 different models were tested respectively. By using the same geometry model with 5 different viscous models according to the results of the analysis; k- ω (sst), laminar and LES analysis of the results has come closer to each other. k- ϵ turbulence model, turbulence within the flow is not fully developed; the pressure values calculated from the others is higher (Table 5.1).

Table 5.1. Different viscous model simulation results

l	(Pa)/Mode	k- ϵ	k-w (sst)	k-w (standard)	Laminar	LES
	P _{in_aorta}	98	60	39	61	56
	P _{in_conduit}	573	363	342	367	359
	P _{aorta_wall}	34	29	28	29	45
	P _{conduit_wall}	117	69	69	70	173

In general, the entire k- ϵ model was calculated in the high turbulence viscosity. Thus, the flow of forces and viscosity values were higher than actual situation. K- ω Standard model, the turbulence viscosity rate on the conduit, aorta-conduit anastomosis and ascending aorta have shown that high. The analysis with k- ω SST model showed the rate of turbulence viscosity on the aorta flow combined with the artificial vascular flow and the aortic arch was high. In the exit from the descending aorta, the speed with which it returned to a uniform rate structure is reduced. These findings in the aorta and the aorta-conduit anastomosis geometry best suited for the analysis of the turbulence model k- ω SST

(transitional) model to be seen. After that, the turbulence model is used in rest of the analysis.

k- ω SST Transitional turbulence model solves Reynolds-averaged Navier Stokes (RANS) equations for the conservation of mass and momentum and 2 additional transport equations for turbulent kinetic energy k and specific dissipation ω (55).

$$\frac{\partial}{\partial t}(\rho k) + \frac{\partial}{\partial x_i}(\rho k u_i) = \frac{\partial}{\partial x_j} \left(\Gamma_k \frac{\partial k}{\partial x_j} \right) + \tilde{G}_k - Y_k + S_k \quad (5.1)$$

$$\frac{\partial}{\partial t}(\rho \omega) + \frac{\partial}{\partial x_i}(\rho \omega u_i) = \frac{\partial}{\partial x_j} \left(\Gamma_\omega \frac{\partial \omega}{\partial x_j} \right) + G_\omega - Y_\omega + D_\omega + \quad (5.2)$$

In equation 5, \tilde{G}_k represents the generation of turbulence kinetic energy due to mean velocity gradients, and in equation 6, G_ω represents the generation of specific dissipation. Γ_k and Γ_ω represent the effective diffusivity of k and ω , respectively. Y_k and Y_ω represent the dissipation of k and ω due to turbulence.

5.4. CFD ANALYSIS

The fluid equations were solved with segregated pressure based implicit method, and all pressure and momentum equations were discretized with 1st order upwind model. The convergence criteria were set to 10^{-3} for residuals.

The operating fluid blood was modeled as Newtonian fluid with a density of 1050 kg/m³ and a viscosity of 0.0035 kg/m-s. The inlet boundary conditions were set as mass flow inlet as 2.5 lt/min for aorta inlet and 5 lt/min for conduit inlet. The aorta outlet boundary condition was pressure outlet, and no-slip boundary condition was applied along the inner walls.

5.4.1. Steady, Constant Mass Flow rate

The steady CFD simulations for each 18 designs were examined in terms of flow streamlines through conduit and aorta, pressure distribution and wall shear stress distribution on artificial artery and aorta wall, and also the numerical results of pressure change, maximum and minimum fluid properties were measured.

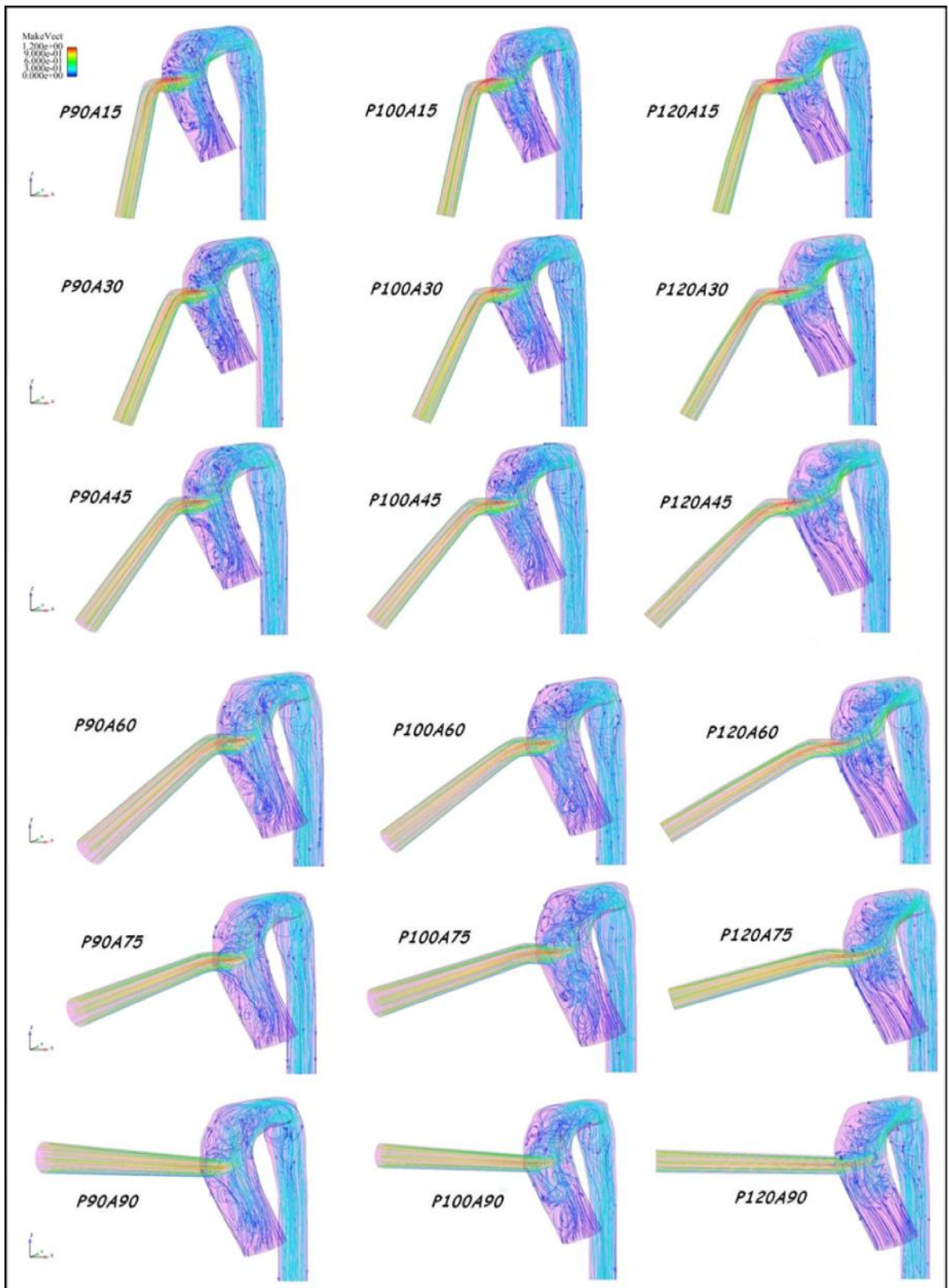


Figure 5.1. Velocity streamlines inside conduit and aorta measured from conduit inlet and aorta inlet

The streamlines were measured from both artificial artery and anastomosis inlet. The blood traveling from conduit inlet to the aorta decomposed into two parts just after the anastomosis location and directed to aortic arch and aortic valves. For the designs modeled by lower connection angles (15° , 30° and 45°), the fluid lost most of its energy at conduit curve so its velocity decreased and the impact effect on the aorta wall was reduced. Thereby, the reverse flows did not seem to be as high as the anastomosis designs modeled with higher connection angles (60° , 75° and 90°).

In addition, the 120° location designs, the blood traveled through the aorta wall from ascending aorta to aortic arch, so that the occurrence of reverse flows to the aortic valves were less than the 90° and 100° location designs (Figure 5.1).

The helical flow profile could be seen through the whole geometry, however from ascending aorta and aortic arch to descending aorta its influence decreased.

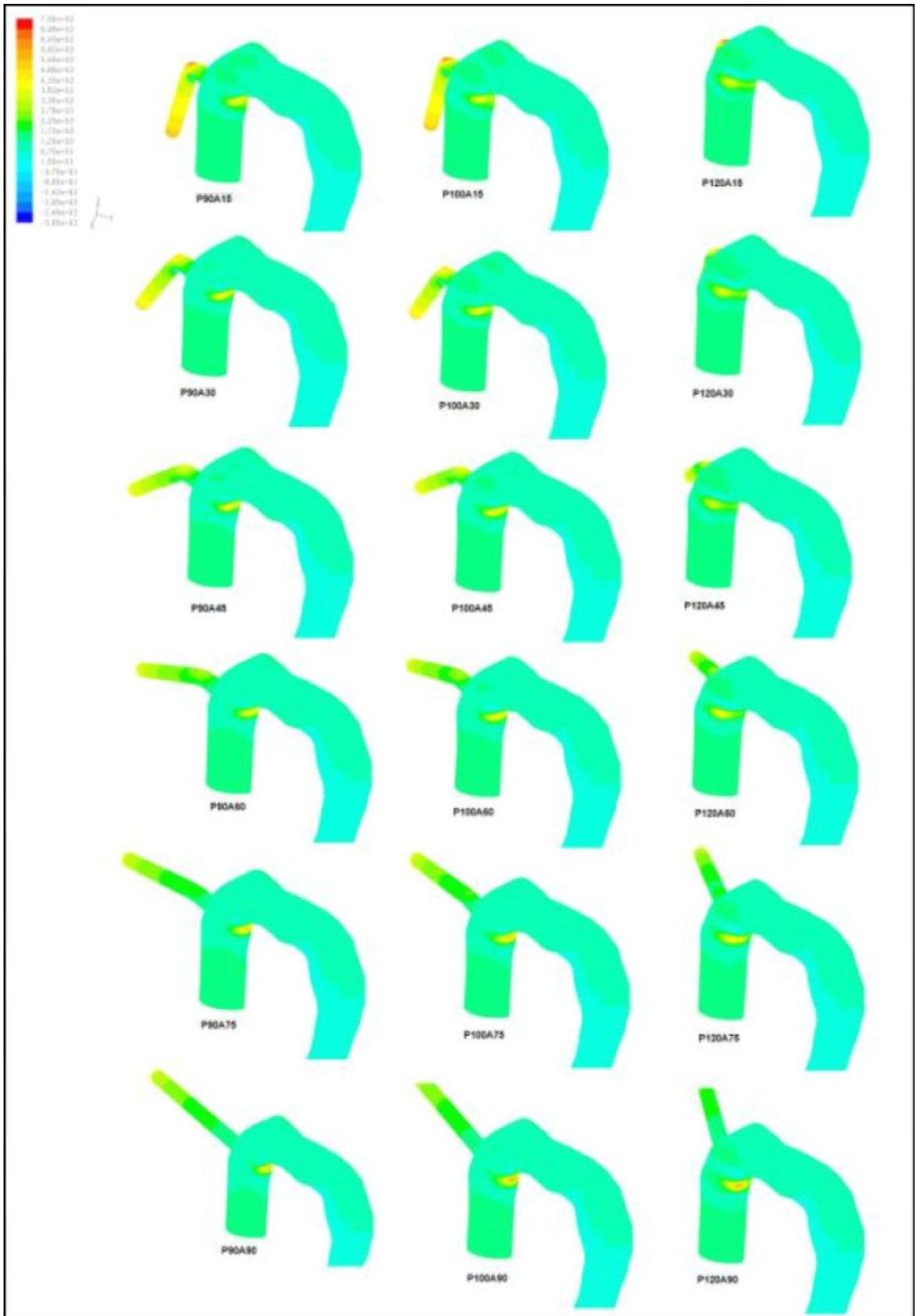


Figure 5.2. Pressure distribution on vessel walls

The flow abnormalities such as reverse flows and helical flows caused increase of pressure and wall shear stress distribution on the artificial artery and aorta wall.

From Figure 5.2, it can be concluded that, for lower connection angles the maximum pressure values were seen on the conduit inflection point, however as the connection angle increased the maximum pressure values occurred on the aorta wall opposite the anastomosis.

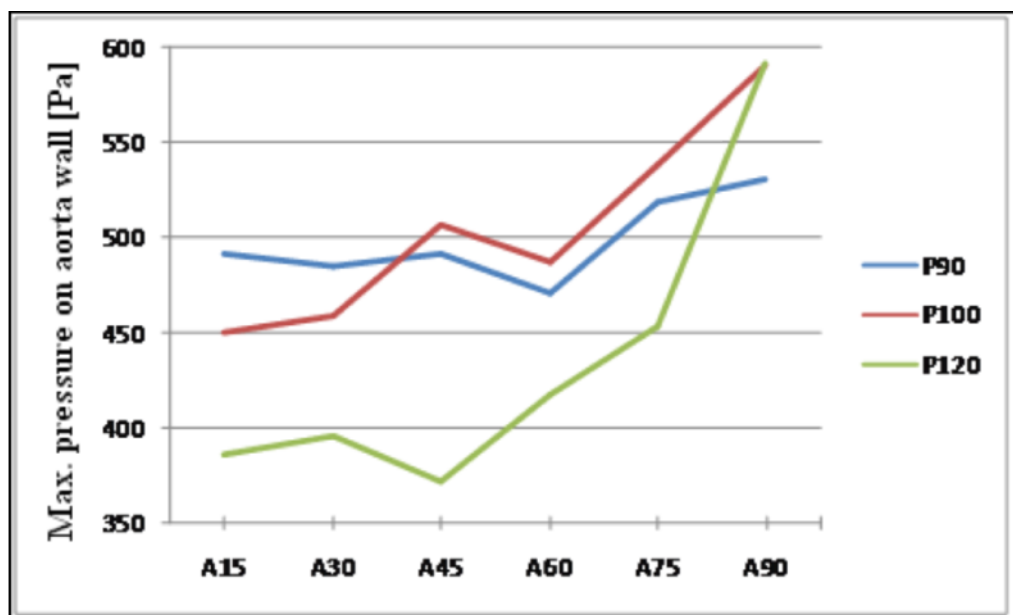


Figure 5.3. Max. pressure value on aorta wall



Figure 5.4. Wall shear stress distribution on vessel walls

The wall shear stress values on the vessel walls showed parallelism with the pressure disturbance, at high pressure values, also the wall shear stress values were high, i.e. on conduit inflection wall with lower connection angles, aorta wall opposite to the anastomosis.

The flow profile was seemed to be uniform on ascending and descending aorta for 120° designs rather than 90° and 100° designs, therefore, the wss values were calculated as 0 on ascending and descending aorta.

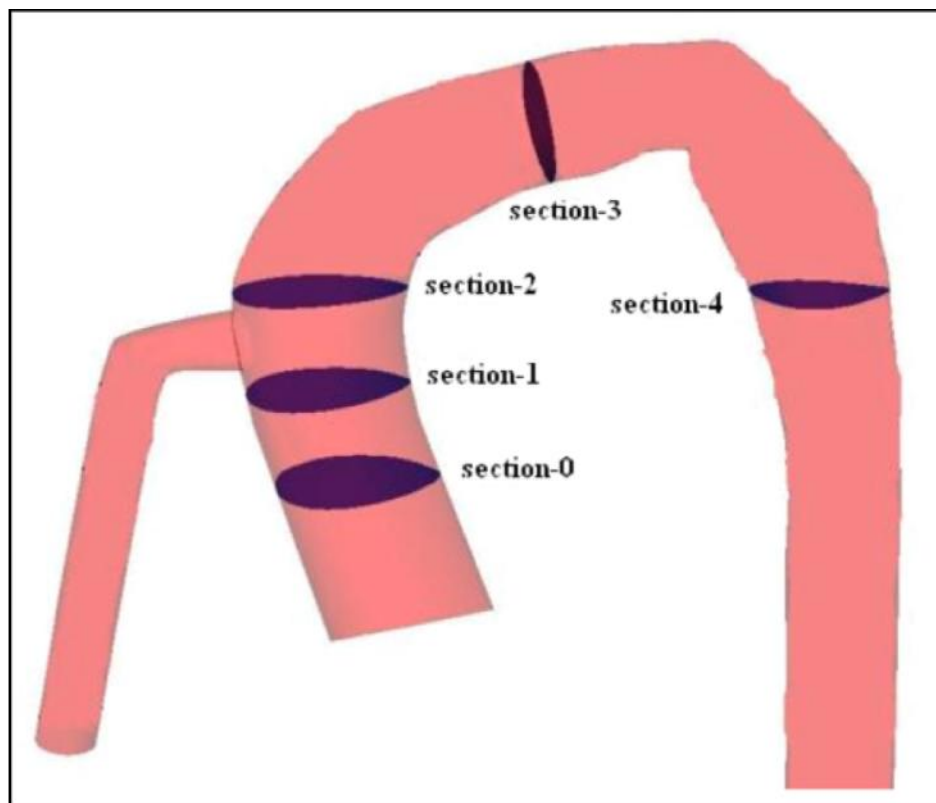


Figure 5.5. Sections

To investigate the effects of the anastomosis position on the secondary flows, 4 different sections were taken perpendicular to the flow direction.

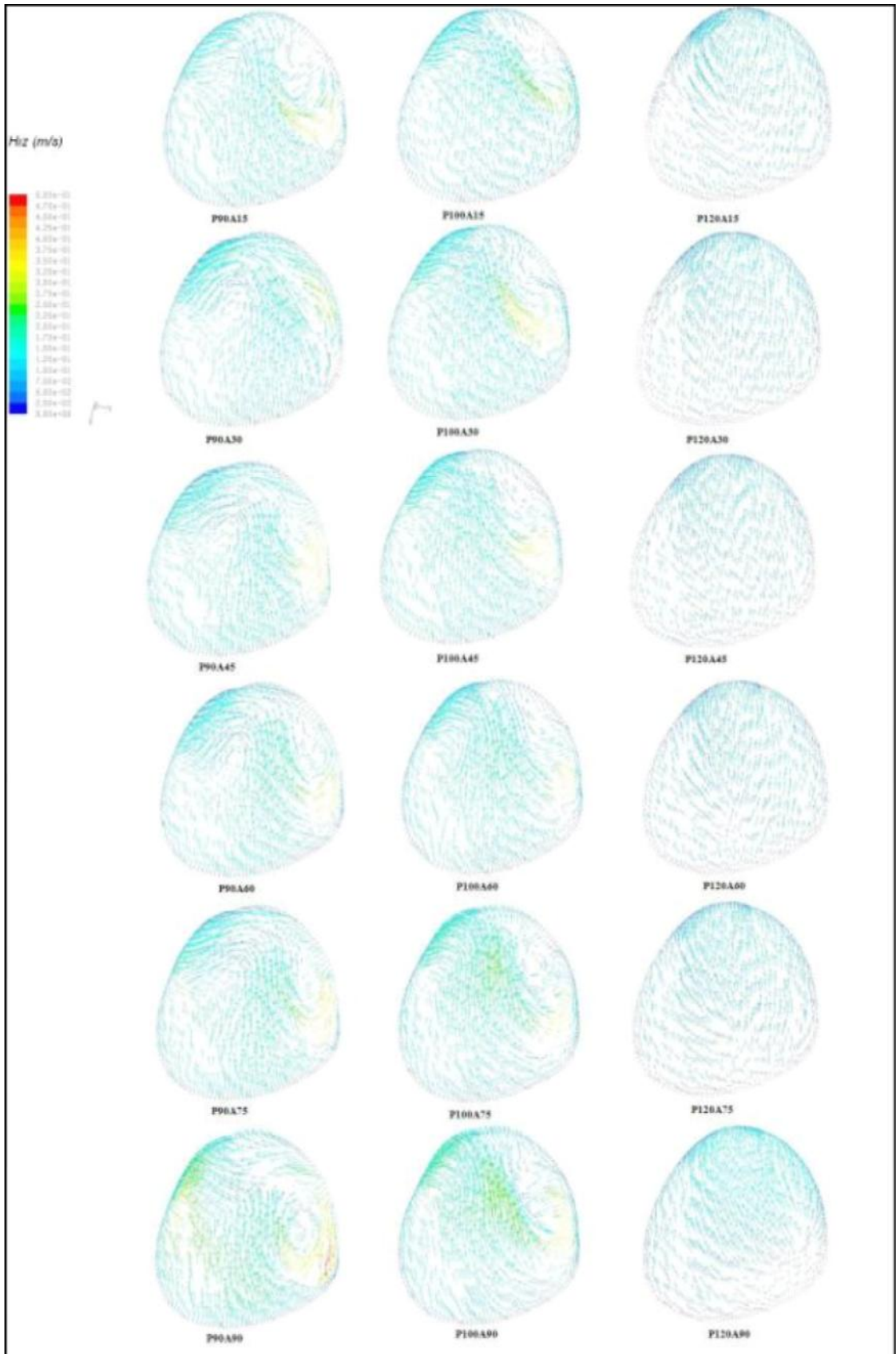


Figure 5.6. Velocity vectors on section-0

The comparison of secondary flows on section-0 was shown in Figure 5.6, in which the section was modeled just above the aortic valves. As mentioned before, the blood flow canalized towards the aortic arch for 120° designs, but the 90° and 100° designs caused a retrograde flow towards the aortic valve, so the secondary flows could be seen on 90° and 100° designs, but there have not seen any that kind of flow for 120° designs yet.

Moreover, on the second section just below the anastomosis position, the secondary flow patterns increased rapidly for 90° and 100° designs, and the new formation of secondary flows could be seen for 120° designs in Figure 5.7.

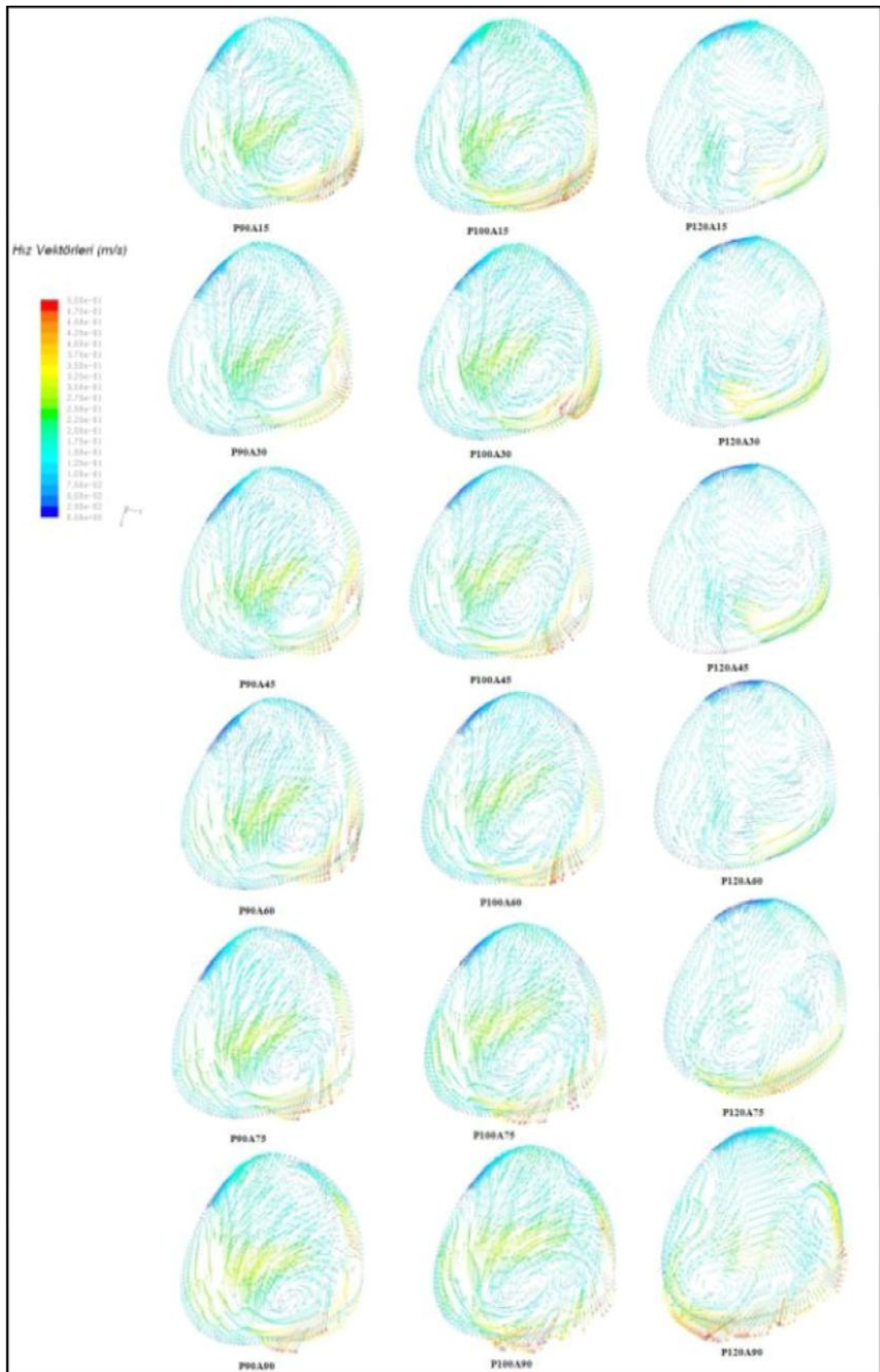


Figure 5.7. Velocity vectors on section-1

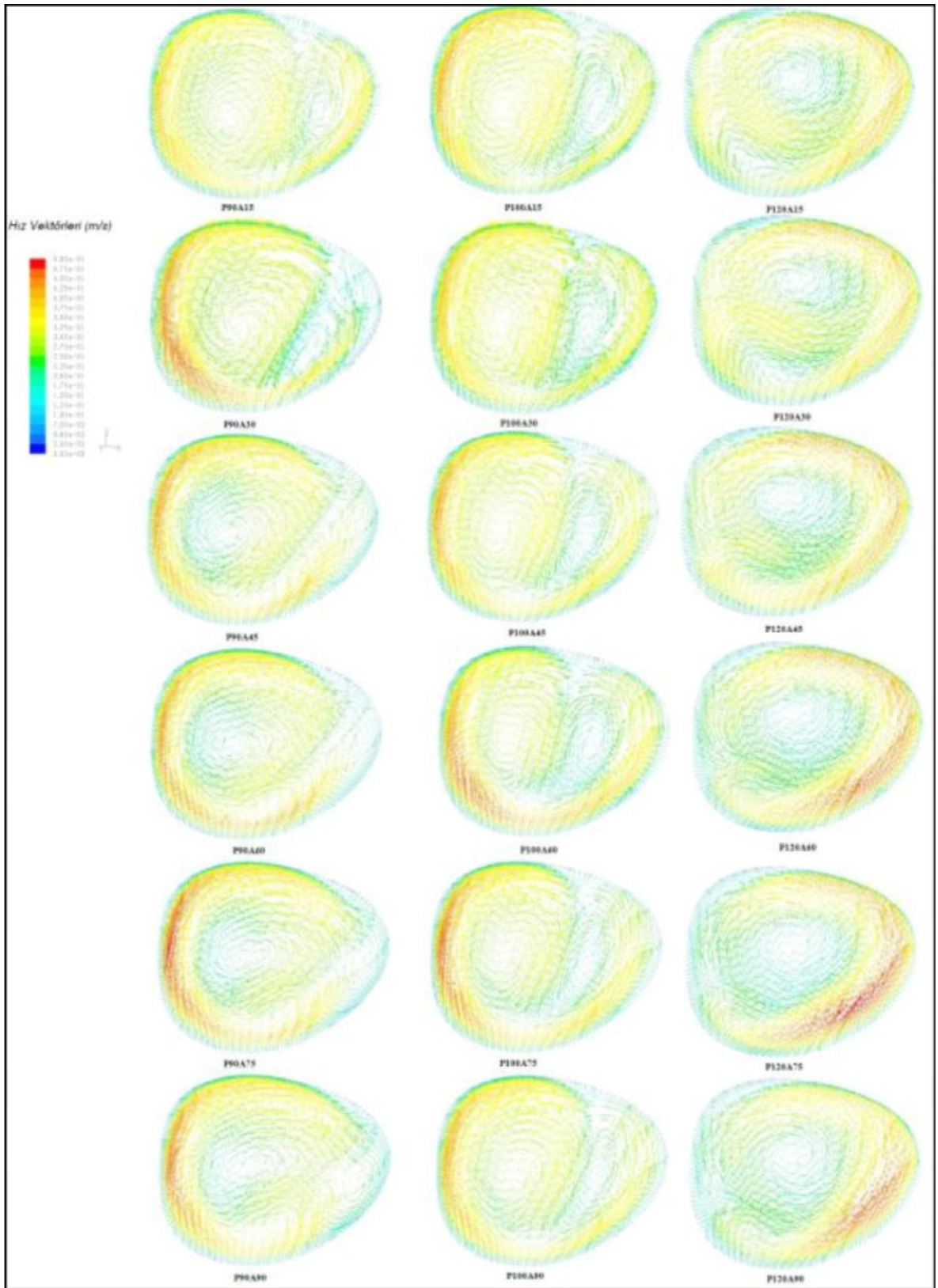


Figure 5.8. Velocity vectors on section-3

In Figure 5.8, the secondary flow patterns were shown on section 3, placed in the middle of the aortic arch. For the each of the 90° and 100° designs, there existed two big secondary flow regions, but for each 120° designs it was limited by one.

On that section for all designs, the measured wss values on the vessel wall were very high; however this value decreased through the descending aorta.

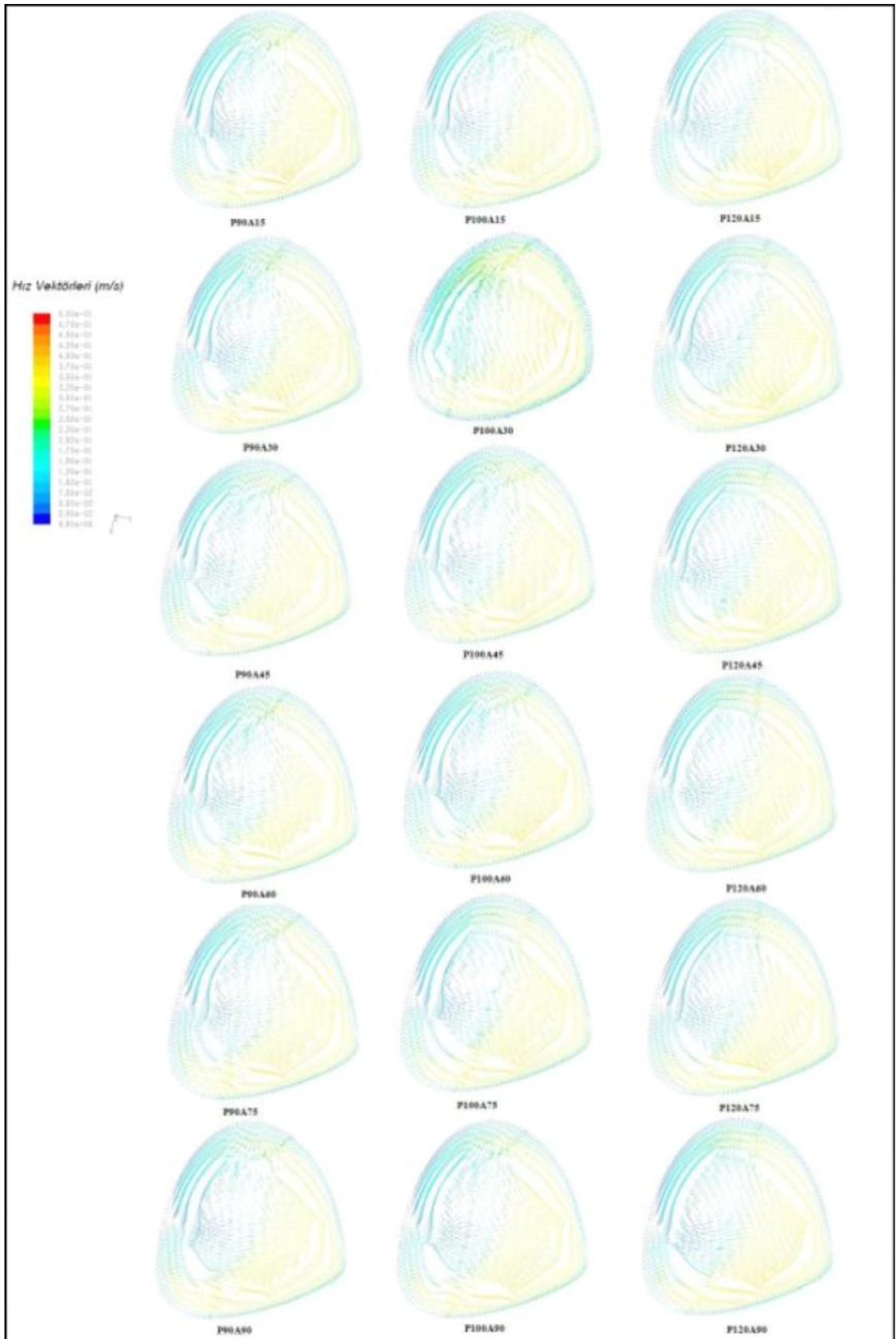


Figure 5.9. Velocity vectors on section-4

5.5. CONCLUSION

The compared results were interpreted in terms of the blood flow structure within the artificial artery and aorta considering the reverse flow formation through the aortic valves, pressure and wss distribution on the vein wall.

Therefore, connecting the conduit with a higher angle to the aorta consists of more pressure and WSS on the aorta wall opposite the place of connection, while the smaller connection angle designs, the fluid loses its speed and flow effect over the bend. For 90° and 100° locations, the fluid is directed to heart valves, as the blood collides to aorta wall at the opposite of the anastomosis position. Nevertheless, the 120° designs, blood moves along the aortic arch, and the collision effect decreases. The lesser the impact effect, the less secondary flow and reverse flow formation. The flow through the ascending aorta has better distribution for 120° designs, as the secondary flows have not occurred on the ascending aorta below the anastomosis position.

In accordance with these results, considering both hemodynamic effects on blood cells and vein walls, and clinical applications, the 120° connection location with 15° connection angle design is seemed to be the most appropriate anastomosis model.

6. LEFT VENTRICLE AND CANNULA

After LVAD implementations, it has been seen that the rested left ventricle gained some of its functioning ability with the help of the body's compensation mechanisms; however, most of the time these partial improvements are not enough. To succeed long life LVAD applications, the left ventricle and cannula connection should be proper, so the investigation of the flow inside the left ventricle and cannula geometry is the other significant part of this study.

6.1. LITERATURE SURVEY

There are many researches about flow inside left ventricle in literature; however as the heart anatomy is very complicated including mitral and aortic valves movements and contraction and relaxation of the heart, most of the studies are started with some assumptions to overcome these difficulties. The flow inside aorta during filling phase, the relation between the blood hemodynamics and the vein wall structure, and the flow through the valves and left ventricle are the high interest subjects of these studies.

6.2. GEOMETRY AND MESH

The aortic valve and mitral valve diameters were modeled as 31 mm and 30 mm respectively. The cannula diameter was 12 mm, and its thickness was 3 mm.

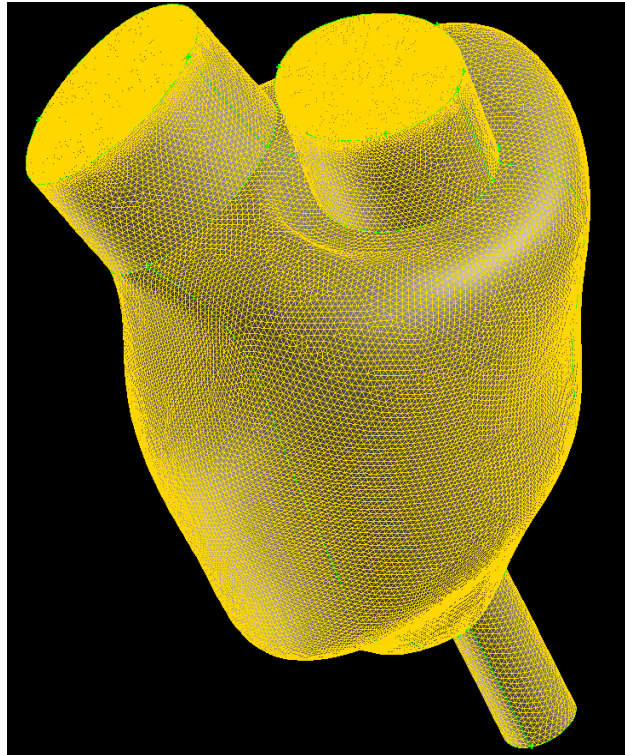


Figure 6.1. Control volume structure for left ventricle and cannula geometry

6.3. CFD ANALYSIS

The first analysis was performed applying the 6 lt/min constant mass flow rate at mitral valve inflow boundary condition, wall boundary condition for aortic valve and pressure outlet boundary condition for cannula outlet. Both the left ventricle and cannula walls were modeled with no-slip wall boundary condition.

6.3.1. Steady, Constant Mass Flow Rate

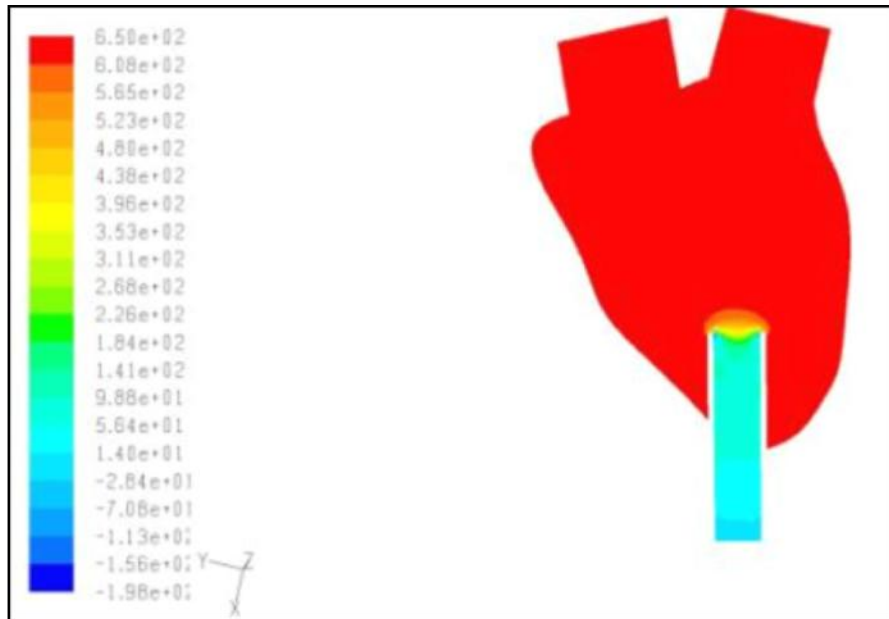


Figure 6.2. Pressure distribution on middle section

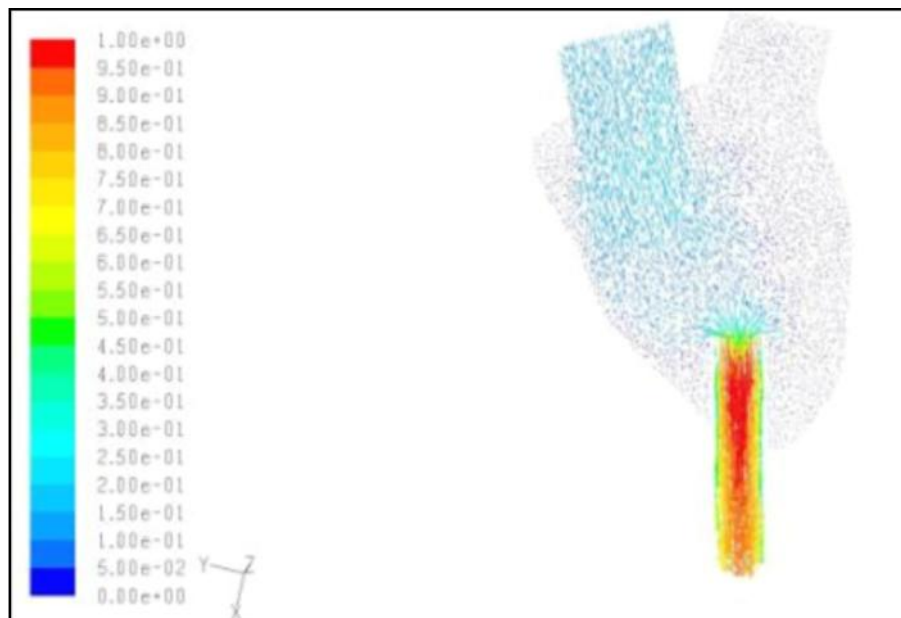


Figure 6.3. Velocity vectors on middle section

In Figure 6.2 and Figure 6.3, the pressure distribution and velocity vectors are shown on a cross section obtained from the center of left ventricle.

6.4. CONCLUSION

When the blood is pumped according to a healthy heart contraction, a large vortex region occurs, especially in the apex region. If the blood is sucked from left ventricle by a pump through the cannula geometry, the stagnant flow regions are formed around the apex of the left ventricle, which can be one of the most important factors triggering the clotting.

REFERENCES

1. *Cardiovascular Diseases*. s.l. World Health Report, 2003-2005.
2. *Can lifestyle changes reverse coronary heart disease? The lifestyle Heart Trial*. Ornish, Dean. s.l. Lancet, 1990, Vol. 336, pp. 129-33.
3. *Intensive lifestyle changes for reversal of coronary heart disease*. D. Ornish, L. W. Scherwitz, R. S. Doody, D. Kesten, S. M. McLanahan, S. E. Brown. s.l. JAMA, 2001, Vol. 280.
4. Maton, Anthea. *Human Biology and Health*. New Jersey Prentice Hall, 1993. ISBN 0-13-981176-1.
5. Gordins, F. S. *Control Theory and Biological Systems*. s.l. Columbia University Press, 1963.
6. *Integrative Cardiovascular Physiology a mathematical model synthesis of cardiac and blood vessel hemodynamics*. Grodins, F. S. s.l. Quart. Rev. Biol., 1959, Vol. 34, pp. 93-116.
7. *Mathematical Model for Fundamental Regulation Processes in the Cardiovascular System*. F. Kappel, R. O. Peer. s.l. J. Math. Biol., 1993, Vol. 31, pp. 611-31.
8. *Patient-specific operative planning for aorta-femoral reconstruction procedures*. N. Wilson, F.R. Arko, C. Taylor. Berlin Medical Image Computing and Computer-Assisted Intervention, 2004. pp. 422-429. 3217.
9. J. R. Cebra, R. Löhner. *From Medical Images to CFD Meshes*. s.l. Institute for Computational Sciences and Informatics, George Mason University, 2000.

10. *Analysis of MR phase-contrast measurements of pulsatile velocity waveforms.* N. J. Hangiandreou, P. J. Rossman, S. J. Riederer,. s.l. Journal of Magnetic Resonance Imaging, 1993, Vol. 3, pp. 387-394.
11. *Numerical simulation of hemodynamics in stented internal carotid aneurysm based on patient-specific model.* Wenyu Fu, Zhaoyong Gu, Xianlong Meng, Bo Chu, Aike Qiao. s.l. Journal of Biomechanics, 2010.
12. *Patient-specific hemodynamic analysis of small internal carotid artery-ophthalmic artery aneurysms.* Aichi Chien, Satoshi Tateshime, James Sayre, Marcelo Castro, Juan Cebral, V. Fernando. s.l. Surgical Neurology, 2009, Vol. 72.
13. D. P. Giddens, T. D. Tang, F. Loth. Fluid Mechanics of Arterial Bifurcations. In Biological Flows. [ed.] C. Caro M. Y. Jaffrin. s.l. Plenum Press, 1995, pp. 51-68.
14. *Pulsatile Flow Visualization in the Abdominal Aorta Under Differing Physiologic Conditions Implications for Increased Susceptibility to Atherosclerosis.* J. E. Moore Jr., D. N. Ku, C. K. Zarins, S. Glagov. s.l. Journal of Biomechanical Engineering, 1992, Vol. 114, pp. 391-397.
15. *Vortex dynamics in a model left ventricle during filling.* Bernardo Baccani, Federico Domenichini, Gianni Pedrizzetti. s.l. European Journal of Mechanics B/Fluids, 2002, Vol. 21, pp. 527-543.
16. *A concentrated parameter model for the human cardiovascular system including heart valve dynamics and atrioventricular interaction.* Theodosios Korakianitis, Yubing Shi. s.l. Medical Engineering & Physics, 2006, Vol. 28, pp. 613-628.
17. *Economic impact of heart failure in the United States Time for a Different Approach.* J. B. O'Connell, M. R. Bristow,. s.l. Journal of Heart Lung Transplant, 1994, Vol. 13, pp. 107-112.

18. *The health care costs of the heart failure in Sweden.* T. Ryden-Beregsten, F. Andersson. 1999 *Journal of International Medicine*, Vol. 246, pp. 275-284.
19. *Computational fluid dynamics as a development tool for rotary blood pumps.* G. W. Burgreen, J. F. Antaki, Z. J. Wu, A. J. Holmes. 25, 2001, *Artificial Organs*, pp. 336-340.
20. *A fluid dynamic analysis of a rotary blood pump for design improvement.* J. Treichler, SE Rosenow, G Damm. 17, 1993, *Artificial Organs*, pp. 797-808.
21. *Effects of Left Ventricle Assist Device support and outflow graft location upon aortic blood flow.* K. N. Litwak, S. C. Koenig, H. Tsukui, S. Kihara, Z. Wu, G. Pantalos. 50, 2004, *ASAIO Journal*, pp. 432-437.
22. *Computational approach for probing the flow through artificial heart devices.* C. Kiris, D. Kwak, S. Rogers, I. D. Chang. 4, s.l. *Journal of Biomechanical Engineering*, 1997, Vol. 119, pp. 452-460.
23. *Computational geometry for patient-specific reconstruction and meshing of blood vessels from MR and CT angiography.* L. Antiga, B. Ene-Iordache, A. Remuzzi. s.l. *IEEE Transactions on Medical Imaging*, 2003, Vol. 22, pp. 674-684.
24. *Computational Fluid Dynamics hemodynamic changes in abdominal aortic aneurysm after stent-graft implantation.* T. Frauenfelder, M. Lotfey, T. Boehm, S. Wildermuth. 4, s.l. *Cardiovascular and Interventional Radiology*, 2006, Vol. 29, pp. 613-625.
25. *Fluid-structure interaction within a layered aortic arch model.* F. Gao, Z. H. Guo, M. Sakamoto, T. Matsuzawa. 5, s.l. *Journal of Biological Physics*, 2006, Vol. 32, pp. 435-454.
26. *Efficient computational fluid dynamics mesh generation by image registration.* D. C. Barber, E. Oubel, A. F. Frangi, D. R. Hose. 6, s.l. *Medical Image Analysis*, 2007, Vol. 11, pp. 648-662.

27. *A three-dimensional, time dependent analysis of flow through a bileaflet mechanical heart valve.* M. J. King, J. Corden, T. David, J. Fisher. 5, s.l. Journal of Biomechanics, 1996, Vol. 29, pp. 609-618.
28. *A multiphysics simulation of a healthy and diseased abdominal aorta.* R. H. McGregor, D. Szczerba, G. Szekely. 2, s.l. Med Image Comput Assist Interv, 2007, Vol. 10, pp. 227-234.
29. *3-D numerical simulation of blood flow through models of the human aorta.* L. Morris, P. DElasus, A. Callanan, M. Walsh, P. Grace. 5, s.l. Journal of Biomechanical Engineering, 2005, Vol. 127, pp. 767-775.
30. Soufer, M. D. Robert. Heart Failure. *Yale University School of Medical Heart Book.* 14.
31. *Scandiatransplant: Thirty years of cooperation in organ transplantation in the Nordic countries.* M. Madsen, P. Asmundsson, I. B. Brekke. 1998 : Clinical Transplantation, pp. 121-131.
32. *Increasing family consent for organ donation: Findings and challenges.* Rocheleau, C. A. s.l. Prog Transplant, 2001, Vol. 11, pp. 194-200.
33. *Particle image velocimetry measurements of blood velocity in a continuous flow ventricular assist device.* S. W. Day, J. C. McDaniel, H. G. Wood, P. E. Allaire, N. Landrot, A. Curtas. 47, 2001, ASAIO Journal, pp. 406-411.
34. *Left atrial vortices studied with 3D phase contrast MRI.* A. Fyrenius, T. Ebbers, L. Wigström, B. Wranne, A. F. Bolger. 3, s.l. Clinical Physiology and Functional Imaging, 1999, Vol. 19, p. 195.
35. *Phase-velocity cine magnetic resonance imaging measurement of pulsatile blood flow in children and young adults: in vitro and in vivo validation.* A. J. Powell, S. E. Maier, T. Chung, T. Geva. s.l. Pediatric Cardiology, 2000, Vol. 36, pp. 104-110.

36. *The importance of imaging assessment before endovascular repair of thoracic aorta.* H. Rousseau, V. Chabbert, M. A. Maracher, O. El Aassar, J. Auriol, P. Massabuau, R. Moreno. s.l. European Society for Vascular Surgery, 2009, Vol. 38, pp. 408-421.
37. *Cardiovascular flow measurement with phase-contrast MR imaging: Basic facts and implementation.* J. Lotz, C. Meier, A. Galanski Leppert, M. s.l. Radio Graphics, 2002, Vol. 22, pp. 651-671.
38. *Blood flow rates by NMR measurements.* JR, Singer. s.l. Science 1959, 1959, Vol. 130, pp. 1652-1653.
39. *Effect of left ventricular assist device outflow conduit anastomosis location on flow patterns in the native aorta.* K. May-Newman, B. Hillen, W. Dembitsky. 52, 2006, ASAIO Journal, pp. 132-139.
40. *Effect of LVAD outflow conduit insertion angle on flow through the native aorta.* K. D. May-Newman, B. K. Hillen, C. S. Sirona, W. Dembitsky. 2004, Journal of Medical Engineering & Technology, pp. 105-109.
41. *3D MR flow analysis in realistic rapid-prototyping model systems of thoracic aorta: Comparison with in vivo data and computational fluid dynamics in identical vessel geometries.* C. Canstein, P. Cachot, A. Faust, A. F. Stalder, J. Bock, A. Frydrychowicz, J. Küffer, J. Hennig, M. Markl. s.l. Magnetic Resonance in Medicine, 2008, Vol. 59, pp. 535-546.
42. *Hemodynamic and clinical considerations in vascular surgery.* D. Whitley, M. Whitley, R. F. Neville. 1, s.l. Anesthesia for Vascular Surgery, 1995, Vol. 13, pp. 1-19.
43. *Hemodynamics in the abdominal aorta: A comparison of in vitro and in vivo measurements.* J. E. Moore Jr., S. E. Maier, D. N. Ku, P. Boesiger. 4, s.l. Journal of Applied Physiology, 1994, Vol. 76, pp. 1520-27.

44. *A grid flow adaptive wall-function method for RANS turbulence modelling.* T. Knopp, T. Alrutz, D. Schwaborn. s.l. Journal of Computational Physics, 2006, Vol. 220, pp. 19-40.
45. G. Medic, G. Kalitzin, G. Iaccarino, E. Weide. *Adaptive wall functions with applications.* Standfor Standfor University.
46. CFD Online. *CFD Online.* [Online]
47. Pedley, T. J. *The fluid mechanics of large blood vessels.* Cambridge Cambridge University Press, 1980.
48. Kreyszig, Erwin. *Advanced Engineering Mathematics.* 8. 1988.
49. *Quantitative 2D and 3D phase contrast MRI: optimized analysis of blood flow and vessel wall parameters.* A. F. Stalder, M. F. Russe, A. Frydrychowicz, J. Bock, J. Hennig, M. Markl. 5, 2008, Magnetic Resonance in Medicine, Vol. 60, pp. 1218-1231.
50. *Concerning thromboembolism associated with left ventricle assist devices.* Gross, D. R. 42, 1999, Cardiovascular Research, pp. 45-47.
51. *Three-dimensional magnetic resonance flow analysis in a ventricular assist device.* M. Markl, C. Benk, D. Klausmann, A. F. Stalder, A. Frydrychowicz, J. Hennig, F. Beyersdorf. 134, 2007, Journal of Thoracic and Cardiovascular Surgery, pp. 1471-1476.
52. *Three-dimensional numerical simulation of blood flow in the aortic arch during cardiopulmonary bypass.* Y. Tokuda, M. Song, Y. Ueda, A. Usui, T. Akita, S. Yoneyama, S. Maruyama. 33, 2008, European Journal of Cardio-thoracic Surgery, pp. 164-167.
53. *The Effect of LVAD Aortic Outflow-Graft Placement on Hemodynamics and Flow.* Biswajit Kar, R. M. Delgado, O.H. Frazier, I. D. Gregoric, M. T. Harting, Y. Wadia,

T. J. Myers, R. D. Moser, J. Freund. s.l. Texas Heart Inst Journal, 2005, Vol. 32, pp. 294-298.

54. *Patient-Specific Isogeometric Fluid Structure Interaction Analysis of Thoracic Aortic Blood Flow due to the Implantation of the Jarvik 2000 Left Ventricular Assist Device.* Y. Bazilevs, J.R. Gohean, T.J.R. Hughes, R.D. Moser, Y. Zhang. s.l. Comput. Methods Appl. Mech. Engrg., 2009.
55. *Two-equation Eddy-Viscosity turbulence models for engineering applications.* Menter, F. R. s.l. AIAA Journal, 1994, Vol. 32, pp. 269-289.

APPENDIX A

The Matlab code and Fluent's UDF were prepared to obtain realistic inflow boundary condition for CFD simulations.

```

% calculations are based on mL/s
% T=1.007 s
T=0;
while(T<5.0350)
for k=1:1:5
i=1;
for p=0:0.01:0.478
f=-
2263995734084255/8589934592*p^5+3368711308697661/17179869184*p^4+31230953
49712877/137438953472*p^3-
5973075751056831/137438953472*p^2+2181707475967647/274877906944*p+83/5
y(i,:)=f;
i=i+1;
end
for p=0.478:0.01:0.744
f=2802863492696409/1099511627776*p^3-
2451510477310591/549755813888*p^2+2765606827113483/1099511627776*p-
1903712437287461/4398046511104
y(i,:)=f;
i=i+1;
end
for p=0.744:0.01:1.007
f=20
y(i,:)=f;
i=i+1
end
end
T=T+0.053;
end
xx = 0 : 0.01 : 1.01;
plot(xx,y)
grid
xlabel('time (s)')
ylabel('flow rate (ml)')
title(Pulsatile flow rate ml/s')

```

Figure A.1. Matlab Code for Lagrange Interpolation formulation